PHYSICAL REVIEW B **85**, 134407 (2012)

Finite-size scaling and boundary effects in two-dimensional valence-bond solids

Anders W. Sandvik
Department of Physics, Boston University, 590 Commonwealth Avenue, Boston, Massachusetts 02215, USA
(Received 14 February 2012; revised manuscript received 20 March 2012; published 3 April 2012)

Various lattice geometries and boundary conditions are used to investigate valence-bond-solid (VBS) ordering in the ground state of an $S = 1/2$ square-lattice quantum spin model—the J-Q model, in which four- or six-spin interactions Q are added to the standard Heisenberg exchange J. Ground-state results for finite systems (with up to thousands of spins) are obtained using an unbiased projector quantum Monte Carlo method. It is found that great care has to be taken when extrapolating the order parameter to infinite lattice size, in particular, in cylinder geometry. Even though strong VBS order exists in two dimensions, and is established clearly with increasing system size on $L \times L$ lattices (or $L_x \times L_y$ lattices with a fixed aspect ratio L_x/L_y of order 1), only short-range VBS correlations are observed on long cylinders (when $L_x \to \infty$ at fixed L_y). The correlation length increases with the cylinder width, until long-range order sets in at a "critical" width. This width is very large even when the 2D order is relatively strong. For example, for a system in which the order parameter is 70% of the largest possible value, $L_y = 8$ is required for ordering. Extrapolations of the VBS order parameter based on correlation functions (the square of the order parameter) for small $L \times L$ lattices can also be misleading. For a 20%-ordered system, results for L up to $\approx$20 appear to extrapolate clearly to a vanishing order parameter, while for larger lattices the scaling behavior crosses over and extrapolates to a nonzero value (with exponentially small finite-size corrections). The VBS order parameter also exhibits interesting edge effects related the known emergent U(1) symmetry close to a "deconfined" critical point, which, if not considered properly, can lead to wrong conclusions for the thermodynamic limit. The observed finite-size behavior for small $L \times L$ lattices and long cylinders is very similar to that predicted for a Z_2 spin liquid. The results therefore raise concerns about recent numerical work claiming Z_2 spin-liquid ground states in 2D frustrated quantum spin systems, in particular, the Heisenberg model with nearest and next-nearest-neighbor couplings. Based on the results presented so far, a VBS state in this system cannot be ruled out.

DOI: 10.1103/PhysRevB.85.134407 PACS number(s): 75.10.Kt, 75.10.Jm, 75.40.Cx, 75.40.Mg

I. INTRODUCTION

A valence-bond solid (VBS) is a state of a quantum spin system in which there is no magnetic long-range order, but lattice symmetries (translational and some times rotational) are broken due to dimerization or, more generally, polymerization of the system into one with a larger unit cell than the underlying lattice. One can think of the spins within a unit cell of a VBS (or within different groups of spins in a large complex unit cell) as having an enhanced probability of forming a total spin singlet. In this paper, manifestations of VBS order in ground states of finite systems are investigated, using unbiased quantum Monte Carlo (QMC) simulations of $S = 1/2$ spins on the two-dimensional (2D) square lattice with interactions—Heisenberg exchange supplemented by certain multispin interactions—leading to columnar order in the thermodynamic limit.[1] The approach to the infinite-size 2D limit is investigated for different boundary conditions. The models considered can be tuned from strong to weak VBS order (and also through a critical point), enabling bench-mark investigations of asymptotics and crossover behaviors. In particular, consequences of near-criticality of the VBS order on the finite-size behavior can be examined in detail. The stability of VBS order on long cylinders ($L_x \times L_y$ lattices with $L_x \gg L_y$) is also addressed. This geometry is often used in density matrix renormalization (DMRG) studies,[2,3] with recent intriguing results pointing to the absence of VBS order and the existence of spin liquids in frustrated models whose ground states have been debated for a long time.[4–6]

In the following introductory sections, several background facts motivating further studies of VBS order are discussed and some of the known properties of VBS states are briefly reviewed. The purposes of the studies reported here will then be detailed, followed by an outline of rest of the paper.

A. VBS states and frustrated interactions

VBS states have been known for a long time to exist in 1D frustrated quantum spin chains. In particular, in the $S = 1/2$ Heisenberg chain with nearest- and next-nearest-neighbor couplings J_1 and J_2, the ground state at coupling ratio $g = J_2/J_1 = 1/2$ is exactly a product of singlets formed on alternating nearest-neighbor bonds (a pattern which can be realized in two different ways; hence the ground state is twofold degenerate).[7] Away from this special, exactly solvable point, there are fluctuations modifying the simple product state. Numerical exact diagonalization studies have shown that long-range dimerization survives down to $g_c \approx 0.241$.[8–10] For $g < g_c$, the ground state exhibits critical spin and VBS correlations (like the standard Heisenberg chain with $J_2 = 0$).[11] At higher g, the simple dimer VBS order persists at least up to $g \approx 0.6$, above which more complicated VBS or spiral spin states likely form.[12,13]

The frustrated 2D square-lattice J_1-J_2 Heisenberg model (with nearest-neighbor couplings J_1 and the J_2-interactions connecting spins across the diagonals of each four-spin plaquette) also has a nonmagnetic ground state in some window of coupling ratios $0.4 \lesssim g \lesssim 0.6$ (outside of which the ground state is Néel antiferromagnetic for smaller g and exhibits stripe

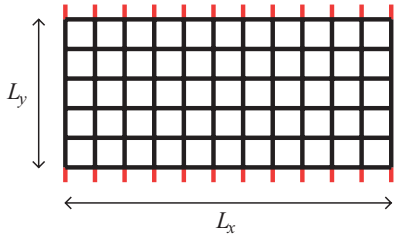

FIG. 1. (Color online) A cylindrical, semiperiodic 2D square lattice with open edges (left and right sides) and periodic boundary conditions in the vertical direction (i.e., the open links at the top and bottom are connected to each other).

antiferromagnetic order for larger g).[14–17] However, in this case, it has been difficult to determine the exact nature of the ground state. Many studies over the past two decades have suggested a VBS, with either columnar or plaquette (four-spin unit cell) order,[15–27] but spin-liquid ground states (which have no broken symmetries but may have topological order)[28] have also been proposed.[14,29] Very recently, results of DMRG calculations on cylindrical semiperiodic lattices (with open edges in one direction—see Fig. 1) were used to argue more specifically that the ground state of the system for $0.41 \leqslant g \leqslant 0.62$ is a Z_2 spin liquid.[6] A concurrent calculation based on tensor-product states also claimed the absence of VBS order.[30]

A story similar to that of the J_1-J_2 Heisenberg model has played out in recent years in the case of the $S = 1/2$ Heisenberg model with only nearest-neighbor interactions on the geometrically frustrated kagome lattice. Many calculations initially suggested a VBS ground state (in this case with a complex 12- or 36-site unit cell),[31–35] but the most recent DMRG studies support a Z_2 spin-liquid scenario[4,5] (as also predicted in early analytical work).[36] Here, as well, cylindrical lattices played a crucial role in obtaining the numerical data.

B. Deconfined quantum-critical points and VBSs with emergent U(1) symmetry

When the Néel order of a 2D antiferromagnet such as the $S = 1/2$ Heisenberg model is destroyed in a continuous quantum phase transition, one scenario is that the putative spin-liquid state is immediately unstable to the formation of a VBS. This has been argued to lead to a "deconfined" quantum-critical point separating the Néel and VBS states.[37,38] The phase transition is associated with deconfinement of spinons. Being generically continuous, due to subtle quantum interference effects, this type of transition violates the classical "Landau rule," according to which a transition between two ordered states breaking unrelated symmetries should be generically first order.

In the low-energy field-theory argued to describe the deconfined quantum-critical point (the $2 + 1$ dimensional noncompact CP^1 theory),[37] the VBS fluctuations correspond to a U(1) gauge field to which spinons are coupled. There is a dangerously irrelevant operator (a quadrupled monopole operator), which reduces the U(1) symmetry to a fourfold (Z_4) symmetry inside the ordered VBS state (in which the spinons become confined). On the square lattice, this corresponds to the four degenerate columnar VBS patterns. Close to the critical point, the Z_4 symmetry only becomes apparent beyond a length-scale Λ, which is larger than the standard correlation length ξ associated with the magnitude of the order parameter. At distances below Λ there are angular fluctuations of the VBS order parameter (D_x, D_y), which in a system with x order, $(|D_x| > 0, D_y = 0)$, induces D_y order on length scales up to Λ, with this length diverging as $\Lambda \sim \xi^{1+a}$ with $a > 0$. At distances much below Λ, the angle of the VBS order parameter fluctuates in an essentially U(1) isotropic manner.

The deconfinement scenario appears to be realized in a class of "J-Q" models,[1,39–43] in which the Heisenberg exchange J is supplemented by certain multispin interactions—products of two or more two-spin singlet projectors acting on different spin pairs. These interactions lead to the formation of local correlated singlets, thereby reducing, and eventually destroying, the Néel order. Results of QMC calculations (which are not affected by sign problems in this case) are consistent with a single critical point separating the Néel state and a VBS. While some works suggested that the transition is weakly first order,[4,95] the most recent studies point to a continuous transition with anomalously large scaling corrections.[41–43] Moreover, emergent U(1) symmetry has been explicitly observed in the VBS order parameter distribution.[1,4] By studying the U(1)-Z_4 crossover, the exponent a was estimated in Ref. 40 to be $a = 0.20 \pm 0.05$.

C. Stability of the spin liquid

For the frustrated spin systems discussed above in Sec. I A, deconfined quantum-criticality, i.e., a gapless spin liquid existing only at a singular point, is also an alternative to the transition out of the Néel state into an extended spin-liquid phase. At the heart of this issue is the question of the stability of the spin-liquid state.[44] The deconfined quantum-criticality scenario implies that some spin liquids are generically unstable, at least under some commonly satisfied conditions, but stable spin liquids can also exist.

Recently Cano and Fendley succeeded in constructing a long-sought local (but complicated) Hamiltonian[45] that is the parent Hamiltonian of the prototypical resonating valence-bond (RVB) spin liquid, i.e., the equal superposition of all nearest-neighbor valence bond configurations (with the Marshall sign rule built in).[46–48] This state, however, is a U(1) spin liquid with exponentially decaying spin correlations but critical VBS correlations,[49,50] and not the kind of fully gapped Z_2 spin liquid proposed in the context of the frustrated models discussed above [but a U(1) spin liquid is also a possible ground-state candidate of this model].[51] As a consequence of its close relationship with the critical Rokhasr-Kivelson dimer model,[49,50] one would expect this state to be generically unstable to perturbations of the Cano-Fendley Hamiltonian, leading to the formation of a VBS. Viewed from the perspective of a class of quantum states, the introduction of longer bonds either maintains the critical VBS,[49] or leads to a Z_2 spin liquid,[52,53] but the Hamiltonian for these extended RVB states is not known.

Stable Z_2 spin liquids are known with Klein Hamiltonians on particular decorated lattices,[54] but the degree of stability of these states when moving away from the limit of high

decoration is not known. The Kitaev honeycomb-lattice model,[55] which has a Z_2 liquid state, can also be related to a model of SU(2) interacting spins on a decorated honeycomb lattice.[56] However, there is still no rigorously known example of a Z_2 spin-liquid ground state of a local SU(2) invariant Hamiltonian on one of the simple standard 2D lattices (square, triangular, honeycomb, kagome, etc). This lack of a prototypical system underlies the quest to find Z_2 liquids in numerical studies of frustrated quantum spin Hamiltonians.[4–6,29,30] Z_2 spin-liquid states have already been confirmed in QMC studies of frustrated quantum XY models.[57]

D. Detection of spin liquids and VBS order

It is highly nontrivial to unambiguously confirm 2D spin-liquid states based on numerical calculations on relatively small lattices. The main difficulty here is to exclude weak VBS order (while the absence of magnetic order is easier to confirm, e.g., by demonstrating a nonzero spin gap). There is therefore much interest in finding positive signals for various spin-liquid phases, e.g., using unique finite-size scaling properties of the entanglement entropy.[58,59] Other signals related to the topological aspects of spin liquids have also been proposed.[6,52] However, regardless of what properties are investigated, great care has to be taken in view of the small lattices accessible for systems with frustrated interactions. Due to sign problems, unbiased QMC studies of the ground states of these systems are essentially impossible[60] (although some progress has been made here recently at elevated temperatures).[61] Variational QMC methods can be used[29,62] but are not reliable, because very different states can have almost the same energy. Exact diagonalization studies can reach ≈42 spins,[63–65] while DMRG calculations now can reach hundreds of spins.[3] Tensor-product state methods (which can be regarded as generalizations of the matrix-product based[66] DMRG scheme) can reach much larger sizes, but are complicated by the fact that extrapolations also have to be carried out in the bond dimension of the tensors.[30,67,68] In DMRG calculations, there is a similar issue with regards to the maximum number of states that can be kept, which is what limits the accessible system sizes (since that number of states in this case has to grow exponentially with the system size).

E. Lattice shapes and boundaries

As already mentioned, in DMRG studies it has become popular to use lattices in the form of cylinders with semiperiodic boundary conditions (with periodic boundaries along the long direction and open short edges), as illustrated in Fig. 1. An aspect ratio $L_x/L_y > 1$ improves the convergence with the number of states kept, as compared to a fully periodic lattice with equal length in both directions (for a given total number of lattices sites).[2] The better convergence with samples of this shape can be traced to the inherently 1D nature of the DMRG procedures and how the generated states can incorporate entanglement.[66] It has also been argued that cylindrical $L_x/L_y > 1$ samples, some times in combination with modifications of the boundaries (e.g., using field terms breaking some symmetry), have other favorable effects as well on the convergence of various order parameters as a function of the system size.[2,3]

In QMC studies of sign-problem free models, periodic $L \times L$ lattices are normally used. In cases where the couplings are spatially anisotropic, it has proved helpful to use $L_x \times L_y$ lattices with $L_x \neq L_y$,[69,70] while in other cases no particular advantages of such rectangular lattices were noted.[10] Open boundaries have been considered in QMC work primarily in cases where the perturbing effects of the edges are the actual targets of investigation.[71,72] In a previous QMC study of a VBS state, it was also noted that open boundaries can be used to break the fourfold symmetry of the 2D VBS completely and stabilize a unique VBS pattern, as an alternative of studying VBS correlation functions in periodic lattices with no explicitly broken symmetries.[73]

F. Purpose of the paper

The main purpose of the present paper is to systematically investigate the role of the lattice shape and boundary conditions on the finite-size scaling properties of the VBS order parameter. VBS states have in the past few years been conclusively demonstrated in several 2D J-Q models,[1,39,40,74,75] and also in 1D chains (where the same kind of dimerization transition takes place as in the frustrated J_1-J_2 chain)[76,77] and 3D systems.[78] Different types of VBS patterns can be realized, depending on the arrangements of the singlet projectors on the lattice. These models have been studied with large-scale QMC simulations, mainly for the purpose of investigating the nature of the Néel-VBS transition.[1,39–43,74,75] Here, the main focus will instead be on the VBS state itself (including its crossover behavior close to criticality), using the J-Q models to obtain generic bench marks for finite-size scaling of this kind of order parameter. An efficient approximation-free ground-state projector QMC method[79,80] was used to obtain results for both strongly and weakly VBS ordered systems on square lattices with different shapes and boundaries.

In order to make contact with the currently favored manner of applying the DMRG method,[2,3] cylindrical systems with open edges in one direction will be studied extensively. The convention adopted here is that the edges parallel to the y axis are open, and periodic boundary conditions are applied in the other direction. Such an $L_x \times L_y$ lattice is illustrated in Fig. 1. In some cases, the open edges will be modified to favor a certain VBS pattern, which is often also done in DMRG studies.[5,6] Fully periodic lattices will also be considered. Two aspect ratios, $L_x/L_y = 1,2$, will be considered for both the semiperiodic and fully periodic systems. The limit $L_x \to \infty$ will also be taken for small L_y.

In addition to suggesting optimal approaches for extracting the VBS order in the 2D thermodynamic limit, the results presented here will also show that the issue of excluding VBS order in a system with an unknown type of nonmagnetic ground state may be more difficult than what has been anticipated so far. In particular, the geometry of long cylinders can give misleading results. Not only can calculations on such systems completely miss 2D VBS order (because the system is disordered with a short correlation length on the cylinders), but also the claimed positive signals of a 2D Z_2 spin liquid[6,52] cannot be trusted when used with cylinders of practically

accessible widths (because they are essentially 1D spin liquids although the state orders in the 2D limit). The emergent U(1) symmetry of the VBS state leads to interesting boundary effects, which are also studied here.

G. Outline of the paper

In Sec. II, the J-Q models are specified in detail, the correlation functions of interest are defined, the projector QMC method is briefly outlined, and its convergence properties are discussed and illustrated with an example. Extrapolations of the infinite-size value of the order parameter is discussed in Sec. III. Results for the J-Q_3 model at $J = 0$ (the pure Q_3 model), which has very robust columnar VBS order, is discussed first, in order to show how the different ways of extrapolating the order parameter to the thermodynamic limit agree well with each other. Results for three different lattice types are compared; periodic $L \times L$ and $2L \times L$ systems as well as semiperiodic cylindrical $2L \times L$ systems. The much weaker VBS ordering in the Q_2 and J-Q_2 models is discussed next, using the same lattices as above. Here, several subtle issues are pointed out that affect extrapolations to infinite size when the order is not strong, and, therefore, the length scales ξ and Λ are large. The quantum-critical scaling form of the VBS order parameter is also discussed, as a nearby critical point also influences the finite-size behavior in systems off criticality. The vector aspects of the columnar VBS order parameter (D_x, D_y) and the effects of its emergent U(1) symmetry are studied in detail in Sec. IV. The evolution of the x and y components of the order parameter as a function of the distance from an open edge is studied, with and without symmetry-breaking modifications of the edge. In Sec. V, the destruction of VBS order on cylinders is studied in the limit $L_x \to \infty$ and L_y fixed. The most important results are summarized and their implications are discussed in Sec. VI. Here, detailed comparisons with the recent DMRG results[6] for the J_1-J_2 Heisenberg model are also made. Detection of the U(1)-Z_4 symmetry of the VBS order parameter based on probability distributions $P(D_x, D_y)$ generated in QMC calculations is discussed in an Appendix.

II. MODELS AND METHODS

A. J-Q models

A generic J-Q model is defined using products of singlet projectors $C(i,j)$ on two sites:

$$C(i,j) = \tfrac{1}{4} - \mathbf{S}_i \cdot \mathbf{S}_j. \tag{1}$$

The standard Heisenberg model is just a sum of such singlet projectors over the interacting bonds $\langle i,j\rangle$ (here nearest-neighbor sites on the square lattice):

$$H_J = -J \sum_{\langle i,j\rangle} C(i,j), \tag{2}$$

where the minus sign corresponds to antiferromagnetic interactions. A Q_n term consists of products of two or more (n) singlet projectors acting on different bonds:

$$H_{Q_n} = -Q_n \sum_a \prod_{b=1}^{n} C(i[a,b], j[a,b]). \tag{3}$$

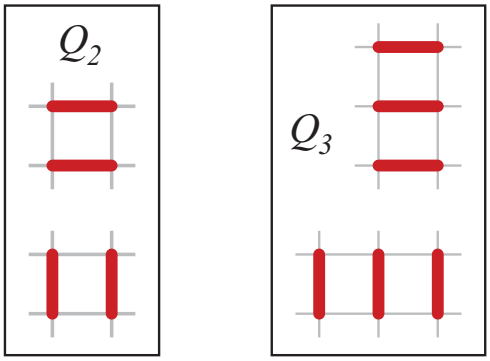

FIG. 2. (Color online) Q_2 and Q_3 terms on the square lattice. The bars of length one lattice constant indicate the locations of singlet projectors $C(i,j)$ on site pairs i,j. The Hamiltonian contains all unique translations of these operators.

Here, a is a label corresponding to the lattice units within which the singlet projectors are arranged and b labels the bonds (spin pairs) on which the singlet projectors within these units act; $i[a,b]$ and $j[a,b]$ above refer to the two sites connected by bond b in unit a. In the simplest kind of Q_2 term on the square lattice, a denotes 2×2 plaquettes with the two projectors within these plaquettes connecting spins either horizontally or vertically (i.e., for a given 2×2 plaquette there are two labels a: one corresponding to horizontal and one to vertical bonds). This standard Q_2 term will be considered here, along with a similar Q_3 term with the projectors arranged in columns. Both these cases are illustrated in Fig. 2. In general, the sum over projectors is such that the Hamiltonian does not break any of the symmetries of the lattice.

The J-Q_n model defined by the Hamiltonian $H = H_J + H_{Q_n}$ hosts a VBS ground state when Q_n/J is sufficiently large. In general, VBS formation is favored for a large enough number n of singlet projectors (with the minimum being typically $n = 2$ or 3 in two dimensions) if the arrangement of them is compatible with some symmetry-breaking pattern of strong and weak bond singlets. In this paper, the pure Q_2 and Q_3 models without any J term will be studied primarily, but some results for J-Q_2 systems with $J/Q_2 > 0$ will also be presented.

B. Projector QMC

J-Q models with minus signs as in Eqs. (2) and (3) do not have QMC sign problems and can be studied with very efficient QMC loop algorithms. Here, the ground-state projector method developed in Ref. 80 is used. It is based on applying a high power of the Hamiltonian to a "trial" state $|\Psi_0\rangle$,

$$|\Psi_m\rangle = (-H)^m |\Psi_0\rangle, \tag{4}$$

where $(-H)^m$ is written as a sum over all possible strings of the individual J and Q terms in Eqs. (2) and (3). Denoting such a string of singlet projectors by $P_m(i)$, with i formally indexing the different strings, an operator expectation value is written as

$$\langle A\rangle_m = \frac{\sum_{ij} \langle\Psi_0| P_m^T(j) A P_m(i) |\Psi_0\rangle}{\sum_{ij} \langle\Psi_0| P_m^T(j) P_m(i) |\Psi_0\rangle}, \tag{5}$$

where $P_m^T(j)$ is the string $P_m(j)$ in reverse order.

The QMC method implements importance sampling of the operator strings $P_m^T(j)P_m(i)$, which is done in two steps, as described in detail in Ref. 80 in the case of the Heisenberg model (and the modifications of the scheme when a Q term is present are straightforward and have been discussed briefly in Ref. 10): first, all the operators in the J and Q terms are split into their diagonal and off-diagonal components in the basis of spin states $|S_1^z,\ldots,S_N^z\rangle$ used. The diagonal operators can be moved around on the lattice as long as each operator is compatible with the spin state on which it acts (with only operations on anti-parallel spins allowed). The full set of operators is sampled by changing the types of some operators from diagonal to off diagonal, or vise versa, on the same lattice unit a, using an efficient loop algorithm.[81–83]

The ground state of a bipartite J-Q model (i.e., with each singlet projector connecting two spins on different sublattices) being guaranteed to be singlet, it is particularly convenient to use a trial state expressed in the valence bond basis in the singlet sector. The convergence of $\langle A\rangle_m$ to the true ground-state expectation value $\langle 0|A|0\rangle_m$ is then dictated by the gap to the second singlet. For a periodic lattice (or a semiperiodic cylinder), a transitional-invariant trial state also filters out excited states with nonzero momentum from the outset. Translational invariance in the applicable lattice direction(s) is easily ensured by using an amplitude-product state[48] for $|\Psi_0\rangle$, i.e., a superposition written in terms of bipartite valence bond states $|v\rangle$,

$$|\Psi_0\rangle = \sum_v c_v|v\rangle. \tag{6}$$

Here, the sum includes all tilings of the N-site lattice into $N/2$ bipartite two-spin singlets, i.e.,

$$|v\rangle = \left|\prod_{i=1}^{N/2}\left(i,j_i^v\right)\right\rangle, \tag{7}$$

where $(i,j) = (|\uparrow_i\downarrow_j\rangle - |\downarrow_i\uparrow_j\rangle)/\sqrt{2}$ with i and j sites on sublattice A and B, respectively, and the weight c_v of a given tiling v into singlets depends only on the "shapes" $\mathbf{l} = (l_x,l_y)$ of the bonds in $|v\rangle$:

$$c_v = \prod_{\mathbf{l}} h(\mathbf{l})^{n_{\mathbf{l}}}, \tag{8}$$

where $n_{\mathbf{l}}$ is the number of bonds of shape $\mathbf{l}$.

Amplitude-product states are very easy to sample in the course of the projection according to Eq. (4), as also described in Ref. 80. The detailed form of the amplitude $h(\mathbf{l})$ is not crucial when the state is used as a trial state. Variationally optimized amplitudes lead to faster convergence with the power m, but even without optimizing the convergence properties are good.[80] In the work reported here, amplitudes decaying with the bond length l as l^{-3} were used (in which case the trial state itself has Néel order, but this is very quickly destroyed by the projection procedure in a VBS state).

C. Correlation functions

In order to characterize the ground state, the spin (s) and dimer (d) correlation functions are computed. These are defined in the standard way as

$$C_s(\mathbf{r}_{ij}) = \langle \mathbf{S}(\mathbf{r}_i)\cdot\mathbf{S}(\mathbf{r}_j)\rangle, \tag{9}$$

$$C_{d\alpha}(\mathbf{r}_{ij}) = \langle B_\alpha(\mathbf{r}_i)B_\alpha(\mathbf{r}_j)\rangle, \tag{10}$$

where $\mathbf{r}_{ij} = \mathbf{r}_i - \mathbf{r}_j$ is the spatial separation of the operators and B_α, $\alpha = \hat{x},\hat{y}$, is the dimer operator on nearest-neighbor bonds oriented in the α direction, e.g., for $\alpha = \hat{x}$

$$B_{\hat{x}}(\mathbf{r}) = \mathbf{S}(\mathbf{r})\cdot\mathbf{S}(\mathbf{r}+\hat{\mathbf{x}}). \tag{11}$$

One can also define cross correlations $\langle B_{\hat{x}}(\mathbf{r}_i)B_{\hat{y}}(\mathbf{r}_j)\rangle$ but they will not be needed here. The correlation functions can be easily computed using loop estimators based on the transition graphs generated when the sampled valence bond states in the ket and bra states of Eq. (5) are propagated by the string of singlet projectors. The estimators are discussed in detail in Refs. 76 and 84.

Columnar and plaquette VBS states can both be detected by the columnar VBS order parameter, which when averaged over the whole lattice of $N = L_xL_y$ sites can be defined by the operators

$$D_x = \frac{1}{N}\sum_{x,y} B_{\hat{x}}(x,y)(-1)^x, \tag{12}$$

$$D_y = \frac{1}{N}\sum_{x,y} B_{\hat{y}}(x,y)(-1)^y. \tag{13}$$

In a columnar state with the lattice rotational symmetry completely broken, either D_x or D_y has a nonzero expectation value, while in a plaquette state they are both nonzero and equal. The J-Q models studied here host only columnar VBS states. However, as we will be discussed below, in a columnar state on a finite lattice one can have both nonzero $\langle D_x\rangle$ and $\langle D_y\rangle$, due to boundary and shape effects.

In periodic and semiperiodic systems where the degeneracy of the possible VBS patterns is not broken, one can only detect the VBS with the corresponding correlation functions, e.g., the squares of the order parameters defined above. In particular, it is useful to consider the total squared order parameter

$$D^2 = D_x^2 + D_y^2. \tag{14}$$

The magnitude of the order parameter in a corresponding symmetry-broken state is $D = \langle D^2\rangle^{1/2}$ (which can be taken as a definition of the value D of the order parameter). In nonsquare samples it is also illuminating to investigate the components $\langle D_x^2\rangle$ and $\langle D_y^2\rangle$ individually, to see how the lattice shape (and boundaries) affects the symmetry breaking. As will be demonstrated in the following sections, this issue is, in fact, of key importance for interpreting numerical results for nonsquare samples.

In the cylindrical semiperiodic systems, it is useful to define the order parameter in such a way that the perturbing effects of the open edges are partially eliminated. As in Ref. 6, for such systems with $L_x > L_y$ the summations in Eqs. (12) and (13) will normally be taken over only the central sites within a square of size $L_y \times L_y$.

In cases when the lattice coordinates (x,y) are needed explicitly in the further discussion of correlation functions

in the later sections, the numbering convention will be $x \in \{0,\ldots,L_x-1\}$ and $y \in \{0,\ldots,L_y-1\}$.

D. Convergence tests

To examine the convergence properties of the projector method, the state (4) after m operations with H can be written in terms of eigenstates $|n\rangle$ of H as

$$|\psi_m\rangle = \sum_n c_n E_n^m |n\rangle, \tag{15}$$

where c_n are the expansion coefficients of the trial state in the energy basis. Assuming that the ground-state energy E_0 is the largest in magnitude, $|E_0| \geqslant |E_n|, \forall n > 0$, which is the case for sure with a Hamiltonian expressed using the singlet projectors (1) and the signs as in Eqs. (2) and (3), an expectation value of an operator A not commuting with the Hamiltonian can be expanded as

$$\langle A\rangle_m = \langle 0|A|0\rangle + 2\langle 1|A|0\rangle \frac{c_1}{c_0}\left(\frac{E_1}{E_0}\right)^m + \cdots. \tag{16}$$

Here, $|1\rangle$ is the first excited state in the symmetry sector considered, which with an amplitude product state obeying all applicable lattice symmetries is a singlet that is fully symmetric with respect to all the symmetry operations (translations, reflections, and rotations of the lattice). With the gap $\Delta = E_1 - E_0$ and a large projection-power m, Eq. (16) can be written as

$$\langle A\rangle_m = \langle 0|A|0\rangle + c\exp\left(-\frac{m}{N}\frac{\Delta}{|e_0|}\right), \tag{17}$$

where e_0 is the ground-state energy per site, $e_0 = E_0/N$, and c is a constant. In order to achieve good convergence, one should therefore use a size-normalized projection power $m/N \gg 1/\Delta$.

The gapped VBS state being of primary interest here, Δ/ϵ_0 approaches a nonzero constant as the system size increases. One may then expect good convergence properties with an essentially size independent m/N. However, for system sizes accessible in practice, the gap still typically decreases significantly with the system size. In addition, the density of states above the gap increases as well. As a consequence, m/N has to be increased with the system size to ensure good convergence. Since the number of operations required for one full sweep of Monte Carlo updates of a configuration in the projector method is of order m,[80] the computation time in practice grows faster than N.

All results presented here were tested for convergence by carrying out several calculations with different projection powers $m/N \propto L$ (with $L = \max[L_x, L_y]$ for nonsquare lattices) and making sure that there is no remaining detectable dependence on m. An example of a detailed convergence test is shown in Fig. 3. Typically, $m/N = L/2$ was sufficient to ensure good convergence. In principle, the singlet-singlet gap can be extracted by fitting the exponential form (17) to data such as those in Fig. 3 (as shown in the inset), but such gaps will not be studied here.

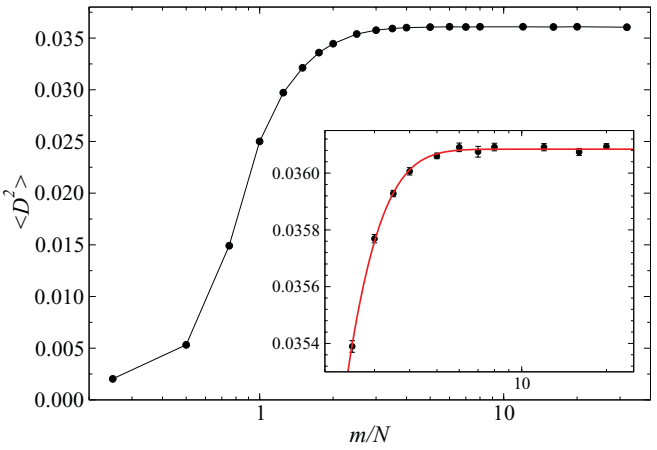

FIG. 3. (Color online) The VBS order parameter as a function of the projection power m (normalized by the system size N) in simulations of the Q_3 model on a periodic 32×32 lattice. The inset shows an exponential fit of the form (17).

III. EXTRAPOLATION OF VBS ORDER

Previous ground-state and finite-temperature QMC studies have confirmed that both the J-Q_2 and J-Q_3 models, with the singlet projectors arranged as in Fig. 2, have VBS-ordered ground states for large Q_n/J.[1,4,39,40] The maximal order parameter obtains for $J = 0$ (pure Q_n models) and, naturally, the order is more robust in the Q_3 model. The previous studies were mainly concerned with the critical and near-critical aspects of the Néel and VBS order parameters—the critical exponents as well as the emergent U(1) symmetry seen in the VBS order parameter (D_x, D_y).

In this section, some important aspects of the VBS order parameter will be discussed first, in particular the expected consequences of its emergent U(1) symmetry. Then, turning to numerical results, the magnitude of the VBS order parameter of the pure Q_3 model will be extracted first, to illustrate the convergence as a function of the lattice size for several cases of lattice shapes and boundary conditions. The J-Q_2 model, including the pure Q_2 case, is then considered in order to investigate potential problems arising when the VBS order is weaker. The quantum-critical scaling will also be discussed briefly, as it is directly related to the extrapolation problems when the VBS can be considered near critical.

A. Nature of the VBS order parameter

Note first that the maximal columnar VBS order parameter is obtained for the state with no fluctuations in the valence bond basis—the state with nearest-neighbor singlets on all bonds of every second column. If the singlets are oriented in the x direction, then the order parameter components defined in Eqs. (12) and (13) have the expectation values $\langle D_x\rangle = 3/8$ (up to an arbitrary sign) and $\langle D_y\rangle = 0$. If the symmetry is not broken and the ground state is an equal superposition of the four degenerate valence-bond states with horizontal and vertical bonds, then the expectation value of the squared VBS order parameter (14) is $\langle D^2\rangle = \langle D_x\rangle^2 + \langle D_y\rangle^2 = 9/64$ in the limit of an infinitely large system. For finite systems, there are corrections to this value, however, which are related to

the nonorthogonality and over-completeness of valence bond states.[49,84]

The emergent U(1) symmetry property of the VBS order parameter[1,37,38,85] and its related length-scale Λ will be of importance in order to understand many of the results to be discussed here and in the later sections. For $L \ll \Lambda$, the order parameter (D_x, D_y) on an $L \times L$ lattice behaves essentially as an isotropic 2D vector, while for $L \gg \Lambda$ the order parameter locks to one of the four angles $n\pi/2$. This is further discussed in the Appendix. Here, for $L_x \neq L_y$ lattices, with or without open edges, the U(1)-Z_4 crossover will manifest itself also in how (on what length scale) the 90° rotational symmetry of the VBS order parameter is broken on a lattice which does not have this symmetry.

It should be noted that symmetry crossovers such as the U(1)-Z_4 case discussed here also occur in many classical systems with dangerously irrelevant perturbations (i.e., ones that do not change the universality class of a phase transitions but reduce the degeneracy of the ordered state), e.g., the 3D XY-model with a q-fold symmetry-breaking field of the form $\cos(q\theta_i)$ (with $q \geqslant 4$).[87,88] There are several numerical studies of the scaling dimension of such a dangerously irrelevant perturbation and the nature of the crossover and its length scale Λ.[89–93]

B. Strong VBS order in the pure Q_3 model

Figure 4 shows the size dependence of $\langle D^2 \rangle$ of the Q_3 model computed on periodic $L \times L$ and $2L \times L$ lattices. For the latter systems, the individual expectation values $\langle D_x \rangle^2$ and $\langle D_y \rangle^2$ are also shown (while these are of course both equal to $\langle D^2 \rangle/2$ for the $L \times L$ lattices). Here, the convergence of $\langle D^2 \rangle$ to a nonzero value when $L \to \infty$ is apparent for both types of lattices. It is interesting to note that both the x and y components are nonzero on the $2L \times L$ lattices for small L, but for larger systems the symmetry is completely broken, eventually leading to $\langle D_x^2 \rangle \to 0$, $\langle D_y^2 \rangle \to \langle D^2 \rangle$. Thus, on the nonsquare periodic lattices, the columnar state with the bonds oriented parallel to the shorter lattice direction (here L_y) is energetically favored. This remains true also for larger aspect ratios L_x/L_y.

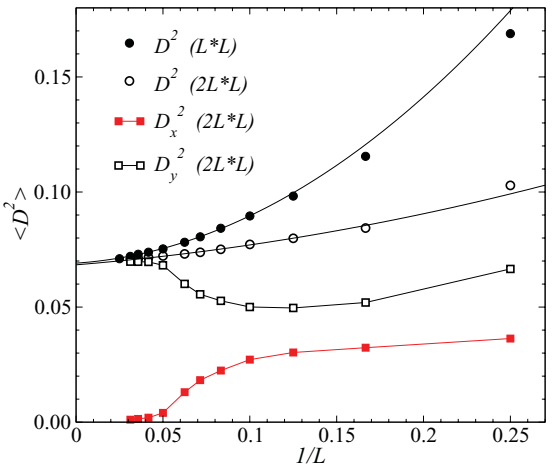

FIG. 4. (Color online) Size dependence of the squared order parameter and its x and y components of the Q_3 model computed on periodic $L \times L$ and $2L \times L$ lattices. The curves passing through the $\langle D^2 \rangle$ data are second-order polynomial fits (excluding the systems for which this form cannot be used). The error bars are much smaller than the plotting symbols (typically the standard deviation is $\approx 2 \times 10^{-5}$).

The crossover from partially broken to fully broken x-y rotation symmetry, which in Fig. 4 takes place for the $2L \times L$ systems for $L \approx 20$, should be related to the emergent U(1) symmetry of the VBS order parameter.[1,37,38] As discussed in the Appendix, for the Q_3 model no perfect U(1) symmetry can be detected on periodic $L \times L$ lattices (since the length-scale Λ is very short), but for a wide range of sizes the system is in a crossover regime between U(1) and Z_4 symmetry. The range of L over which the crossover to a purely y-ordered VBS takes place in Fig. 4 is roughly where all traces of U(1) symmetry vanish on the $L \times L$ lattices (as discussed in Appendix).

Turning now to the quantitative behavior of the total order parameter for the largest systems in Fig. 4, as expected the order parameters for both lattice types extrapolate to the same value in the thermodynamic limit. Fits of the data for the largest systems to second-order polynomials are shown. Note, however, that this form is strictly not correct. For a discrete broken symmetry one would expect the asymptotic finite-size corrections to be exponentially decreasing with increasing system size. It is not easy to reach sufficiently large systems to observe this behavior, however. The second-order fits look reasonably good on the scale of the plot, but in fact they are not of high quality statistically when 6–8 data points are included. Including higher powers helps somewhat, but this can lead to fitted forms that do not behave monotonically as $1/L \to 0$. Such problems with the polynomial fits reflect a crossover to the eventual exponentially rapid convergence. Using second-order fits for the largest few system sizes still should result in a reasonably accurate extrapolated order parameter. Normally, such an extrapolation should give a lower bound on the actual value, but this cannot be guaranteed in the presence of statistical errors. In the case considered here, the results for $L \times L$ and $2L \times L$ extrapolate to 0.0691 and 0.0684, respectively, with the fits shown in Fig. 4. Because of the issues with the, strictly speaking, wrong form of the fitting function, it is not meaningful to compute error bars on these numbers—the purely statistical errors are smaller than the variations among fits with different polynomials and number of data points included. For the purposes of the investigations in this paper, the issue of statistical errors is only of minor importance, however (while the systematical errors due to a wrong fitting form are important).

Data for cylindrical $2L \times L$ systems are shown Fig. 5. Here, the order parameters are computed on the central $L \times L$ square. In sharp contrast to the fully periodic $2L \times L$ systems, here it is the x component of the order parameter that survives in the thermodynamic limit. Thus, the open edges along the y direction favor the bonds ordering perpendicularly to them, and this effect wins over the competing effect, demonstrated in Fig. 4, of the aspect ratio $L_x/L_y > 1$ favoring bonds ordering in the y direction. Quadratic fits to $\langle D^2 \rangle$ and $\langle D_x^2 \rangle$ for a few of the largest system sizes extrapolate to 0.0685 and 0.0694, respectively, in good agreement with the results for the periodic systems.

As a consequence of the open boundaries inducing an x-oriented VBS, the ordering pattern in this case is

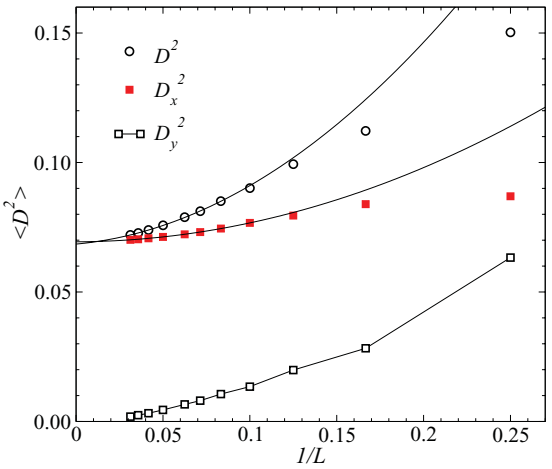

FIG. 5. (Color online) Size dependence of the squared order parameters of the Q_3 model on cylindrical $2L \times L$ lattices (using the central $L \times L$ square for computing the expectation values). The smooth curves are second-order polynomials fitted to the $\langle D^2 \rangle$ data for several of the largest system sizes.

nondegenerate. Therefore the unsquared order parameter $\langle D_x \rangle$ is nonzero and should, in the thermodynamic limit, take a value agreeing with the squared order parameters extracted above; $\langle D_x \rangle \to \langle D^2 \rangle^{1/2}$. The expectation value of the nearest-neighbor spin correlator (11) indeed oscillates considerably as a function of the location along the x direction, as shown in the inset of Fig. 6 for the 32×16 cylinder. The dimer order is clearly the strongest at the edges but remains large also in the interior of the system.

A local VBS order parameter for a system with bonds ordered along the x axis can be defined as

$$D_x(x) = \langle B_x(x,y) \rangle - \tfrac{1}{2} \langle B_x(x-1,y) + B_x(x+1,y) \rangle, \tag{18}$$

which is independent of y on the semiperiodic cylindrical lattices (and can be averaged over y in the QMC calculations).

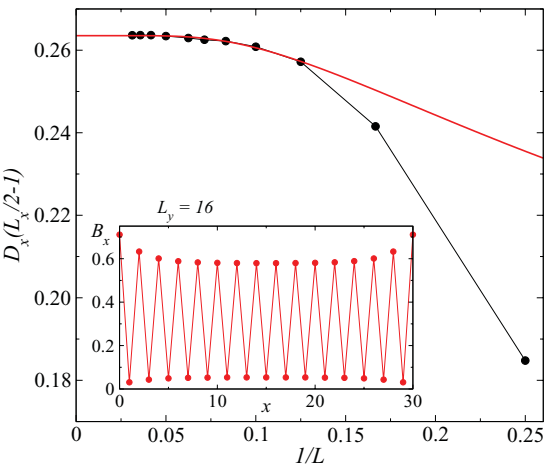

FIG. 6. (Color online) Local columnar x order parameter (18) of the Q_3 model computed at the center of a $2L \times L$ cylinder. The smooth curve is of the exponential form (17) and extrapolates to 0.264. The inset shows the location dependent bond correlation function $\langle B_x(x) \rangle$ for a 32×16 system.

This quantity at the central column is shown as a function of the inverse system size in the main plot of Fig. 6. Here, an asymptotic exponentially fast convergence can be seen clearly, which is illustrated with a fit to the form (17). This fit is of good statistical quality and extrapolates to 0.264, in good agreement with the values for $\langle D^2 \rangle^{1/2}$ obtained above. The magnitude of the order parameter of the Q_3 model is, thus, 70% of the largest possible value (3/8) for a columnar VBS.

C. Reduced order in the Q_2 and J-Q_2 models

In the pure Q_2 model, the VBS order is considerably weaker than in the Q_3 model. The first study of this model gave the order parameter $D \approx 0.070$, or about 20% of the maximal value, based on extrapolations of $L \times L$ results for $L \leqslant 32$.[1] While this order may still be regarded as quite strong, problems with extrapolating it correctly based on small to moderate lattice sizes already start to become apparent.

Figure 7 shows results for periodic $L \times L$ systems with $4 \leqslant L \leqslant 72$. A fifth-order polynomial can be fitted very well to all these data and extrapolates to 0.0063, about 10% lower than the previous result. However, if only $L \geqslant 20$ data are used, a second-order polynomial is sufficient and the extrapolated value is significantly lower: $\langle D_x^2 \rangle = 0.0058$. This illustrates the fact that polynomial fits based on small systems are not very reliable, because of the eventual exponential convergence (which is not yet fully apparent for the system sizes accessible). The resulting relative uncertainties are much larger than in the strongly ordered Q_3 model. The extrapolated value depends significantly on what system sizes are included in the fit and the order of the polynomial used. For the system sizes studied here, a pure exponential form does not yet work.

An important aspect of the finite-size scaling behavior in the Q_2 model is that the data for small to moderate lattices do

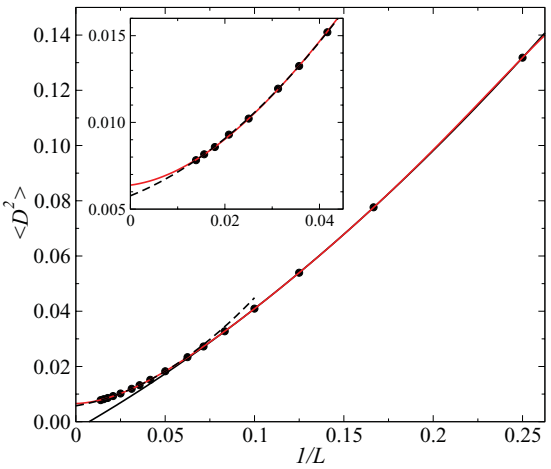

FIG. 7. (Color online) Size dependence of the squared VBS order parameter of the pure Q_2 model on periodic $L \times L$ lattices. The solid black curve in the main graph shows a fit of the $L \leqslant 12$ data to a second-order polynomial (which extrapolates to an unphysical negative value when $L \to \infty$). The solid red curve shows a fifth-order polynomial fit to all the data, while the dashed black curve shows a quadratic fit to only the $L \geqslant 20$ data. The inset shows the behavior for the largest systems on a more detailed scale.

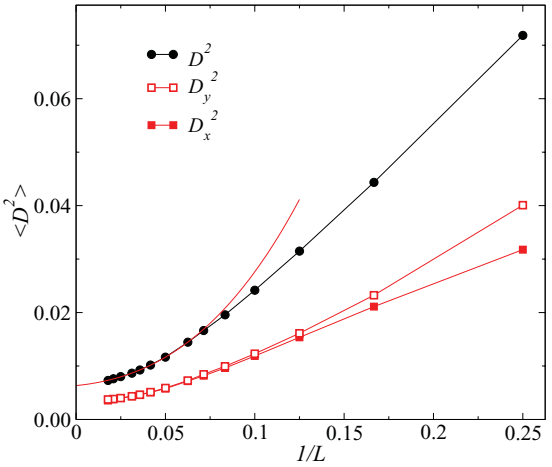

FIG. 8. (Color online) Size dependence of the squared total VBS order parameter $\langle D^2 \rangle$ and its individual x and y components of the pure Q_2 model on fully periodic $2L \times L$ lattices. The curve displayed for $1/L \leqslant 0.125$ is a 4th order polynomial fit to the $\langle D^2 \rangle$ data for $L \geqslant 16$.

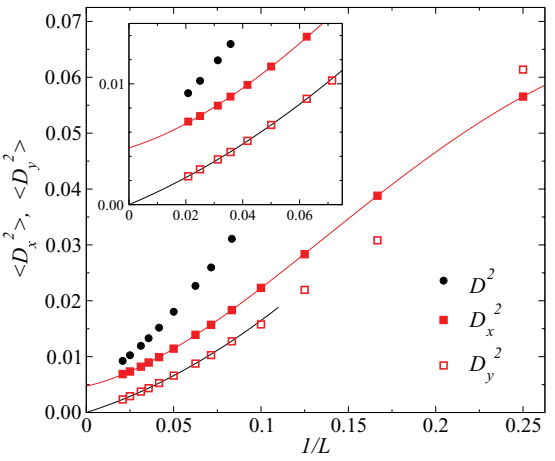

FIG. 9. (Color online) Size dependence of the squared total order parameter $\langle D^2 \rangle$ and its x and y components, computed for the Q_2 model on cylindrical $2L \times L$ lattices (including only the spins on the central $L \times L$ square in the definition of the order parameters). The curves are polynomial fits. In the case of D_y^2, no constant term was included. The inset shows the data for large systems on a more detailed scale.

not even clearly point to an ordered ground state. Figure 7 also shows a second-order fit to only the $L \leqslant 12$ data points. The fit is statistically sound, but extrapolates to a negative value. Without access to larger system sizes it is not possible, using fitting procedures like this in $1/L$, to determine whether the ground state of the infinite 2D lattice is ordered or disordered. At least $L = 20$ is needed with $1/L$ extrapolations to definitely conclude that the ground state is ordered. It can be noted that an asymptotic $\propto 1/L^2$ behavior is expected if there is no long-range order, but this form should apply only for L much larger than the correlation length. Note that the correlation length itself is also not easy to extract from the correlation functions unless $L \gg \xi$ (which is not the case here).

Figure 8 shows results for periodic $2L \times L$ lattices. Using polynomials to reliably extrapolate results to the infinite-size limit is again difficult. An example, using a fourth-order polynomial with data for $L \geqslant 16$ is shown which extrapolates to $\langle D^2 \rangle = 0.0063$. Here, it is again clear that the polynomial is not the correct form, because the fitted curve deviates significantly for the smaller systems not included in the fit.

The behavior of the individual x and y components in Fig. 8 appears to be qualitatively different from that observed in the Q_3 model (see Fig. 4). In the more strongly ordered Q_3 model, the y component is always significantly larger than the x component, and for large systems it completely dominates (the x component vanishing). In the Q_2 model, the length scale Λ of the crossover from U(1) to Z_4 symmetry is much larger, and the dimer order parameter acts as an essentially isotropic vector even for the largest lattices considered here. A crossover to a behavior where the x component vanishes (as in the Q_3 model) should take place for larger system sizes, but, according to the analysis for $L \times L$ lattices in the Appendix, the crossover length is beyond what can currently be studied with QMC calculations, with there being only weak signals of a columnar state. Since the two components are almost equal in magnitude in Fig. 8, not knowing about the peculiar finite-size effects due to emergent U(1) symmetry one may draw the erroneous conclusion from these data of the system being a plaquette VBS.

It is interesting to note in Fig. 8 that the emergent x-y symmetry is not manifested yet for the smallest systems. This reflects the fact that the continuous angular nature of the VBS order parameter only appears upon coarse-graining and $L < 10$ is not sufficiently large for representing a continuous VBS angle. The two crossover length scales, into and out of an U(1) symmetric order parameter, have been investigated in detail in classical systems (clock models) exhibiting emergent U(1) symmetry.[92]

As in the Q_3 model, on the open-edge cylinders with $L_x > L_y$ the favored VBS ordering pattern is that with the bonds primarily in the x direction. Figure 9 shows results for $2L \times L$ cylinders. Here, the effect of the edges to strongly favor x ordering overcomes the tendency to U(1) symmetry, and there is never any size range for which the x and y components are almost equal. Also here the behavior of both components for small lattices exhibit a naive extrapolation to a negative order parameter. For larger lattices $\langle D_x^2 \rangle$, crosses over to a form extrapolating clearly to a nonzero value, while the y component extrapolates to zero. A fourth-order polynomial fit to all the x-component data gives $\langle D_x^2 \rangle = 0.0047$. This is significantly lower than the value quoted above for the examples of extrapolations of $L \times L$ data. However, the extrapolation is again sensitive to the lattice sizes included and the form of the fitting function used.

It is also useful to examine the long-distance VBS correlation function, which should contain less finite-size corrections to the infinite-size order parameter than the sums over all correlations. The squared order parameter (14) contains significant nonasymptotic contributions from short distances. Using the real-space dimer correlation function defined in Eq. (10), the staggered part in the case of the x component (and an analogous form for the y component) can be extracted

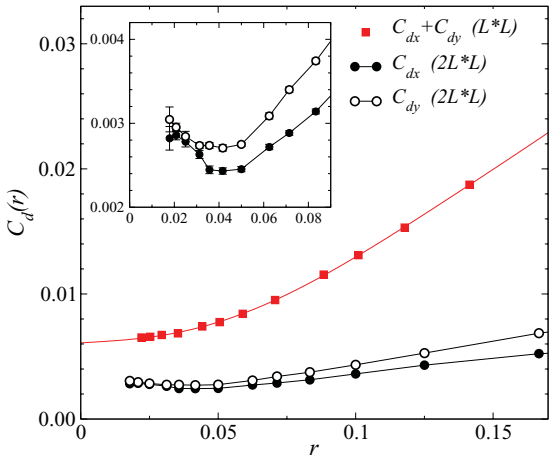

FIG. 10. (Color online) Staggered component, Eq. (19), of the long-distance dimer correlations in the Q_2 model on periodic $L \times L$ and $2L \times L$ lattices. Here, r is the longest distance on the lattices; $\mathbf{r} = (L_x/2, L_y/2)$. The curve through the $L \times L$ data is a high-order polynomial fit. The inset shows the $2L \times L$ data on a more detailed scale.

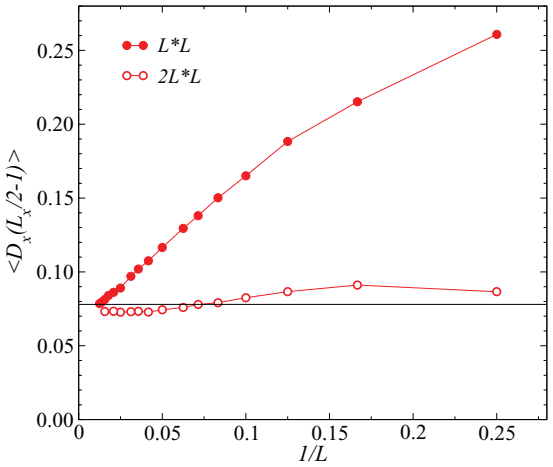

FIG. 11. (Color online) Open-edge induced order parameter of the Q_2 model at the center of cylindrical $L \times L$ and $2L \times L$ lattices. The horizontal line corresponds to the value of the infinite-size order parameter from the extrapolation in Fig. 10.

according to

$$C^*_{dx}(x,y) = \tfrac{1}{2}C_{dx}(x,y) - \tfrac{1}{4}[C_{dx}(x-1,y) + C_{dx}(x+1,y)], \quad (19)$$

where a factor $1/2$ has been included in order for $C^*_{dx}(x \to \infty, y) \to \langle D_x^2 \rangle$, with D_x defined in Eq. (10), in the thermodynamic limit. Figure 10 shows results for the longest distance on periodic $L \times L$ and $2L \times L$ lattices. For the $L \times L$ systems the sum of the x and y components is shown, along with a high-order polynomial fit that extrapolates to the infinite size order parameter $D^2 = 0.0061$. This extrapolation should be reasonably reliable, because the data for the largest systems flatten out clearly, reflecting the asymptotic exponential convergence (unlike the integrated quantity $\langle D^2 \rangle$ in Fig. 7, where no flattening-out is yet seen). For the $2L \times L$ system no reliable extrapolation is possible, because both components exhibit nonmonotonic behavior. The sum of the x and y correlations for large L is nevertheless very close to the $L \times L$ results.

It can also be noted in Fig. 10 that the individual components of the correlation function at long distance show somewhat less prominent x-y symmetry than the integrated correlators in Fig. 8, although they are both still roughly equally large. Again, in the thermodynamic limit one of the components, likely the x component, will have to turn down over and vanish, as the $L_x > L_y$ geometry favors ordering in the y direction.

In the previous section, it appeared that the most reliable way to extract the order parameter in the thermodynamic limit is to exploit the symmetry-breaking open edges, using $\langle D_x(x) \rangle$ defined in Eq. (18). Figure 11 shows such results for open-edge cylinders of size $L \times L$ as well as $2L \times L$. Here, the induced x order appears to extrapolate to a value below the one obtained in Fig. 10 based on the long-distance correlation function—for the $2L \times L$ systems $\langle D_x(L-1) \rangle$ is almost size independent for the largest systems, and one might hence conclude that it has converged. The square of this value is $\langle D_x \rangle^2 \approx 0.073^2 \approx 0.053$, which seems too low compared to the results in Fig. 10.

The reason for this apparent inconsistency should again be related to the emergent U(1) symmetry of the VBS order parameter; in addition to the x component of the order parameter induced by the open edges, there still remains, for the accessible lattice sizes, a non-negligible y component. This component is not locked-in by symmetry-breaking boundaries, however, but averages to zero if measured without first taking the square of its operator. The existence of a non-negligible fluctuating y component nevertheless reduces the induced $\langle D_x \rangle$ from the full value, which should satisfy $D^2 = \langle D_x \rangle^2 + \langle D_y^2 \rangle$ for large systems. It is only when the system size exceeds the U(1) length scale Λ that one can expect the full order parameter to condense into the component $\langle D_x \rangle$, and this length scale cannot at present be reached for the Q_2 model. This shows again that the problem of extracting the VBS order parameter in the thermodynamic limit is a very delicate one.

The examples shown here demonstrate that, when the VBS order is relatively weak (the length scale Λ is large), it is important to look at the full order parameter, including both the x and y components. The long-distance correlation function (see Fig. 10) on $L \times L$ periodic lattices seems to be the fastest converging quantity, and it is in most cases best to use $L \times L$ lattices for extrapolations.

When turning on the Heisenberg exchange J, the VBS order of the J-Q_2 model is reduced and vanishes when $J/Q_2 \approx 0.045$.[41] Here two cases are considered, $J/Q_2 = 0.03$ and 0.10, with the latter corresponding to a near-critical Néel state. Figure 12 shows results for the total squared VBS order parameter and the staggered part of the dimer correlation function (19) averaged over the x and y directions. With $\langle D^2 \rangle$ graphed versus $1/L$ it is again difficult to extrapolate to infinite size based on small lattices. Here, the lattices are nevertheless sufficiently large for it to be apparent that the system at $J/Q_2 = 0.03$ is VBS ordered, while for $J/Q_2 = 0.1$ the decay is much more rapid and consistent with no VBS order. The corresponding long-distance correlations show these behaviors much more clearly, with the $J/Q_2 = 0.03$ data exhibiting the expected exponentially fast convergence to a nonzero value for the largest sizes. Still, if data only for L up to $\approx$10 were

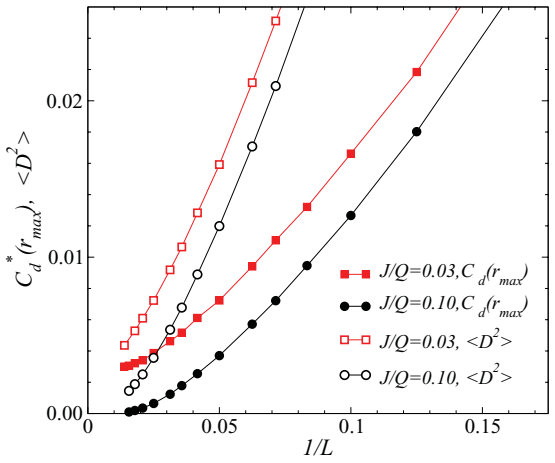

FIG. 12. (Color online) The staggered part, Eq. (19), of the long-distance correlation function (at $r_{\max} = \sqrt{2}L$) and the total dimer order parameter for the J-Q_2 model at $J/Q_2 = 0.03$ and 0.10 on periodic $L \times L$ lattices.

available, it would not be possible to unambiguously confirm the presence of long-range VBS order, even though the order parameter here is still above 10% of the maximum value.

Note that the long-distance correlation function decays exponentially as a function of $1/L$ in a non-VBS state, i.e., much faster than the $1/L^2$ behavior of the total squared order parameter. It is therefore also much easier to confirm the absence of long-range order by studying the long-distance correlations.

D. Quantum-critical scaling

Ultimately, the difficulties in extrapolating the VBS order parameter to infinite size based on small systems will in many cases be related to critical scaling in the proximity of a quantum-critical point (or "pseudo-critical" scaling in cases where the transition out of the VBS state is weakly first order). A small system exhibits quantum criticality also slightly away from the critical point. Hence data for a series of lattices may appear to extrapolate to a disordered state, even though the infinitely large 2D system is on the VBS side of a quantum phase transition. According to conventional finite-size scaling theory, the window around the critical point within which a system of linear size L exhibits scaling is proportional to $L^{-1/\nu}$, where ν is the exponent governing the divergence of the correlation length. Depending on the prefactor, this window may be sizable for practically reachable lattice sizes. As will be shown next, this is one reason why fits to small-lattice data can give misleading results, e.g., in the case of Q_2-model results in Fig. 7.

In addition to illustrating the near-critical VBS, the scaling of the Néel order parameter will also be briefly discussed here. According to past studies, both the J-Q_2 and J-Q_3 models are strong candidates[1,40] for the deconfined quantum-criticality scenario,[37] according to which both order parameters should be critical exactly at the same point. Results for the J-Q_2 model will be discussed here.

While all numerical results so far are consistent with a single Néel-VBS transition point, it has proved remarkably difficult to

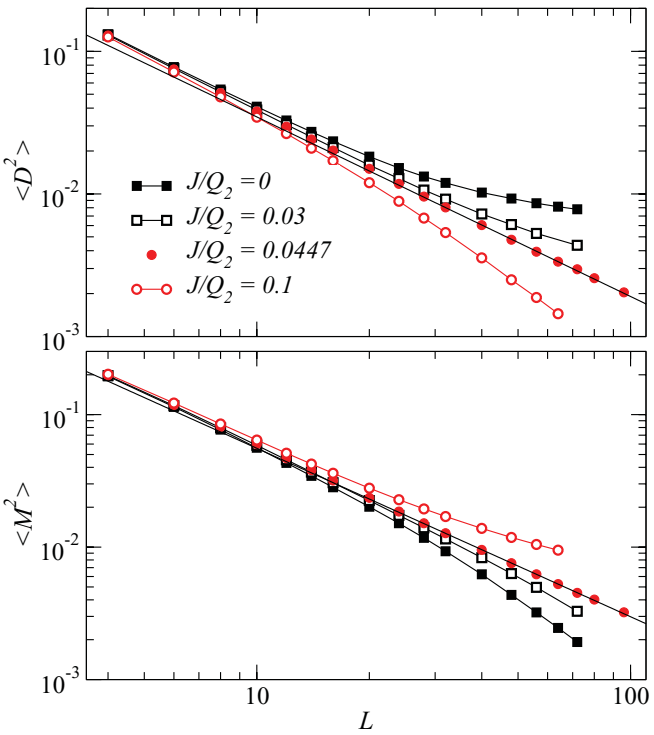

FIG. 13. (Color online) Size dependence of the VBS (top) and Néel (bottom) order parameters of the J-Q_2 model at four different coupling ratios. The point $J/Q_2 = 0.0447$ should be very close to the quantum-critical value according to the scaling analysis of the spin stiffness carried out in Ref. 41. The straight lines fitted through the $J/Q_2 = 0.0447$ data (for system sizes $L \geqslant 32$) have slope -1.27 in both cases.

determine the location $(J/Q_2)_c$ of this transition precisely. The most recent QMC studies point to a continuous transition with unusually large scaling corrections in the quantities normally used to extract the critical point, e.g., the spin stiffness and Binder cumulants.[41–43] These corrections have made it difficult to reliably extrapolate the critical coupling ratio $(J/Q_2)_c$ to infinite size. By using a logarithmic scaling correction to the spin stiffness (which was not predicted in the original field-theory description of deconfined quantum-critical points but may appear with a modified action),[96] $(J/Q_2)_c = 0.0447 \pm 0.0002$ was obtained in Ref. 41. Using a conventional correction $\propto L^{-\omega}$, with small ω and a large prefactor (which potentially could be a consequence of the dangerously irrelevant operator responsible for the Z_4 symmetric VBS), gives a similar result.

In Fig. 13, the two order parameters are graphed versus the system size on log-log scales for coupling ratios close to the critical value. The Néel order parameter $\langle M^2 \rangle$ (the squared sublattice magnetization) is the size-normalized (π,π) Fourier transform of the spin correlation function (9). Both order parameters indeed exhibit critical scaling at $(J/Q_2) = 0.0447$. For other couplings the curves fan out in the way typical for critical points.

Interestingly, at $J/Q_2 = 0.0447$ both order parameters scale as $L^{-(1+\eta)}$ with $\eta \approx 0.27$ (with a purely statistical error bar of about 0.01) when $L \leqslant 32$ systems are used in the fits. For the sublattice magnetization, this exponent is slightly smaller than in previous works,[39,40] while the VBS

exponent is somewhat larger than in Refs. 1 and 40. If these exponents are truly exactly the same, it would imply a duality of the effective low-energy field theory that had not been anticipated,[37] but further detailed work, using larger system sizes and studying several coupling ratios in the neighborhood of $J/Q_2 = 0.0447$, will be required before such a claim can be made (and it could also be a coincidence that the two exponents are almost equal). Note also that the value of η quoted here may also still be affected by subleading scaling corrections.

For coupling ratios larger than the critical value, in Fig. 13 exemplified by $J/Q_2 = 0.1$, the VBS order parameter turns downward, reflecting the faster decay to zero. Asymptotically, in the Néel state, the decay should follow the $1/L^2$ form, but this can only be observed when the lattice size exceeds the correlation length (which is very large this close to the critical point). The sublattice magnetization turns upward, reflecting an extrapolation to a nonzero value. For smaller J/Q_2, here 0 and 0.03, the behavior is the opposite, reflecting a VBS state with no coexisting VBS order.

For the present purpose of detecting VBS order, an important aspect of the critical scaling is that, once a critical point has been identified, upward deviations from the power-law scaling, as seen in Fig. 13 at $J/Q_2 = 0$ and 0.03, still can demonstrate an ordered state when moving away from criticality. It may be easier, in many models, to establish a critical point (or a first-order transition) than to accurately extrapolate the infinite-size value of the order parameter in a state with significant fluctuations (an order parameter significantly smaller than its maximum possible value). Based on the knowledge of the existence of a phase transition, it may be possible to establish long-range order even in the presence of strong quantum fluctuations. This will be the case especially in calculations limited to much smaller systems.

IV. BOUNDARY SYMMETRY BREAKING

One interesting aspect of the results presented in the previous section, exemplified in Figs. 4 and 5, is that the boundary conditions dictate which of the order parameter components, $\langle D_x^2\rangle$ or $\langle D_y^2\rangle$, is the one surviving in the thermodynamic limit. For 90° rotationally symmetric periodic $L \times L$ lattices, both order parameters are of course equal by symmetry (and spontaneous symmetry breaking in the thermodynamic limit will randomly select one of the directions), but in other cases only one of them should survive in the thermodynamic limit (i.e., the lattice shape acts like a symmetry-breaking field). Exactly how the symmetry is broken should be model dependent, and also dependent on fine details of the boundary conditions. Note that there are no "neutral" boundaries for a VBS, i.e., any boundary conditions should favor one component of the order parameter above the other (expect perhaps for some unusual fine-tuned boundaries with adjustable couplings).

Here, the Q_2 and Q_3 models will be used to illustrate the complexity of the boundary issues further, with direct measurements of the order-parameter components $\langle D_x\rangle$ and $\langle D_y\rangle$ in systems where the edges break either the x-translational symmetry or both the x and y symmetries. The boundary effects are particularly interesting in view of the emergent U(1) symmetry, due to which both order parameter components can survive up to large system sizes, as already shown in Sec. III B in the case of periodic systems. Here, the ability of boundaries to twist the local order parameter in the (D_x, D_y) plane will be studied.

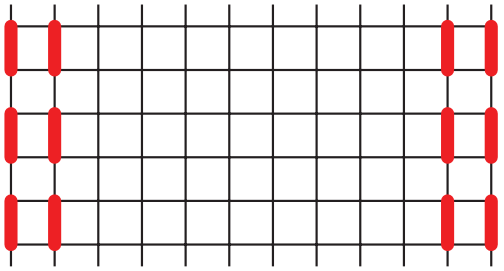

FIG. 14. (Color online) A cylindrical lattice with modified open edges favoring columnar VBS order with vertical bonds. The thick vertical bars represent Q_2 terms *excluded* from the summation in the Hamiltonian, Eq. (3).

Two types of $2L \times L$ cylindrical lattices will be used. In addition to the case discussed so far, where the y-oriented edges are open and uniform, a modified boundary that breaks the translational symmetry in the y direction will also be studied. The modification acts as a field inducing D_y order at the edges. It is interesting to observe the interplay of this effect and the competing effect of the open boundary to lock in D_x ordering when L_x is even (as demonstrated in Fig. 6). This aspect of the VBS ordering is also important in view of DMRG studies, where modified boundaries are often used.[3,5,6] Here, the boundary modification will simply be accomplished by *excluding* from the Hamiltonian the Q_2 or Q_3 terms with vertical bonds closest to an edge on every second row, as illustrated in Fig. 14 in the case of Q_2 terms. Results obtained with only one of the edges modified will be compared with the case of both edges modified in the same way.

The local variations of the VBS vector order parameter (D_x, D_y) of the J-Q_2 model were previously investigated for $L \times L$ lattices with all open edges.[72] The formation of a vortex-like structure in the order parameter was noted. In the cases studied here, there is still translational symmetry with period two along the y axis and, therefore, a 1D description of the order parameter as a function of the x coordinate suffices. The local x and y order parameters are defined using the dimer operator $B_{\hat{x}}$ in Eq. (11);

$$D_x(x) = \big[\langle B_{\hat{x}}(x,y)\rangle - \tfrac{1}{2}\langle B_{\hat{x}}(x-1,y)\rangle - \tfrac{1}{2}\langle B_{\hat{x}}(x+1,y)\rangle\big](-1)^x, \tag{20}$$

$$D_y(x) = [\langle B_y(x,y)\rangle - \langle B_{\hat{x}}(x,y+1)\rangle](-1)^y. \tag{21}$$

These quantities are independent of the y coordinate (and an average is taken in the simulations to improve the statistics). A VBS angle $\theta(x)$ can also be defined,

$$\theta(x) = \mathrm{atan}\left[\frac{D_y(x) + D_y(x+1)}{2D_x(x)}\right], \tag{22}$$

such that $\theta = 0$ and $\theta = \pi$ for a fully x or y oriented VBS order, respectively. The reason for using the sum $D_y(x) + D_y(x+1)$ in the numerator under atan() is that an x-oriented column of bonds labeled by x is located between the y-oriented columns at x and $x+1$ (although such a detail of the definition

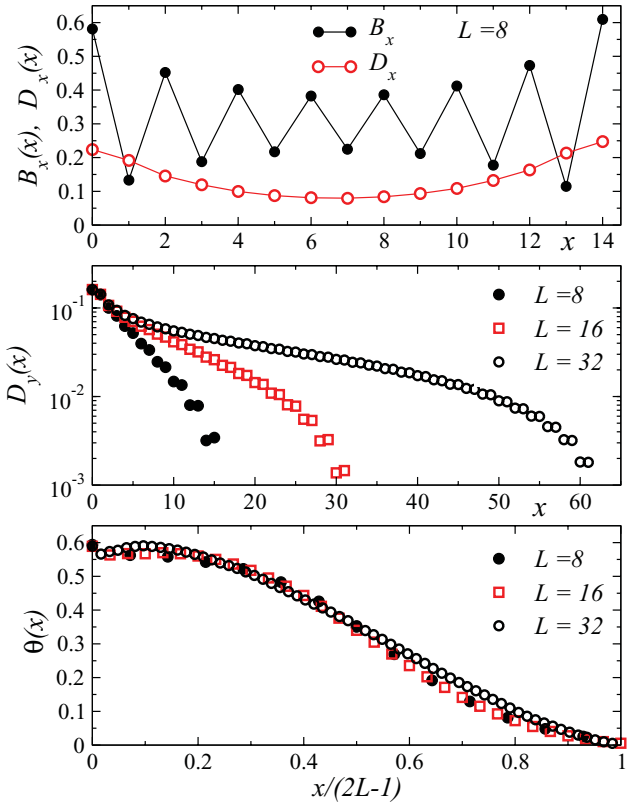

FIG. 15. (Color online) Location-dependent expectation value of the VBS order parameter of the Q_2 model on $2L \times L$ cylinders with the left ($x = 0$) edge modified by the symmetry-breaking perturbation (inducing y-oriented order) illustrated in Fig. 14. The right edge is kept uniform. The top panel shows both the bare dimer expectation value $\langle B_{\hat{x}}(x)\rangle$ and the dimer order parameter $\langle D_x(x)\rangle$ extracted from it according to Eq. (20) for $L = 8$. The middle panel shows the y order parameter defined according to Eq. (21) for $L = 8, 16$, and 32. The bottom graph shows the VBS angle extracted from the x and y order parameters according to Eq. (22).

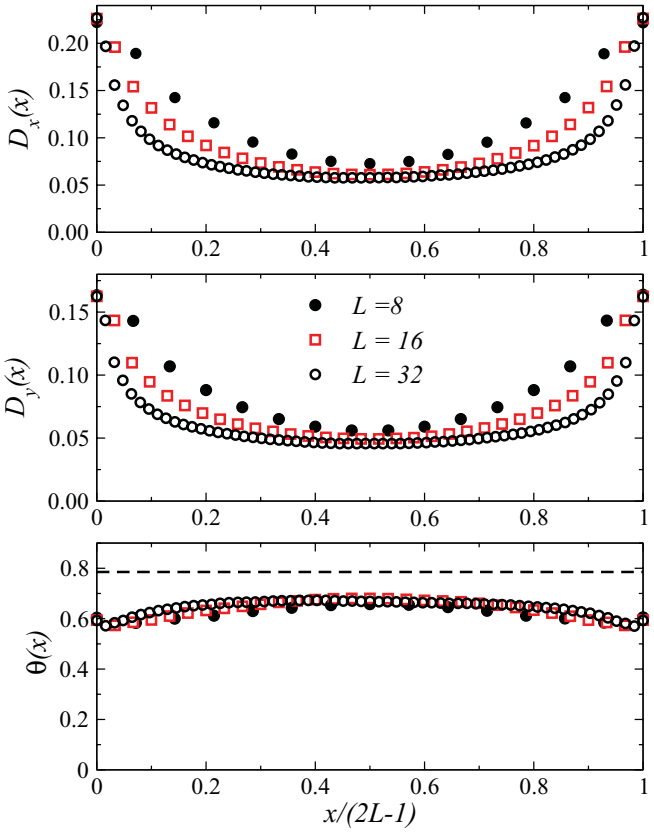

FIG. 16. (Color online) Location dependent expectation values of the x and y VBS order-parameter components, Eqs. (20) and (21), of the Q_2 model on $2L \times L$ cylinders with both edges modified by a symmetry-breaking perturbation (favoring y-oriented bond order). The corresponding VBS angle extracted using Eq. (22) is shown in the bottom panel. The horizontal dashed line is at $\Theta = \pi/4$ (corresponding to equal x and y order parameter parameters).

of the local angle is not strictly important, and there are other equally good definitions giving the same result for large systems).

Figure 15 shows results for the Q_2 model with only one modified edge. Oscillations in the bare dimer expectation value $\langle B_{\hat{x}}(x)\rangle$ are present (top panel) as in the case of the uniform edge in Fig. 6. In this case, however, the function is not reflection symmetric, due to the unequal left and right edges of the cylinder. The order parameter $D_x(x)$ is the largest at the edges. Away from the edge it decays toward a value at the center of the system which is somewhat smaller than the locked-in order parameter previously extracted based on the data in Fig. 9 (which can be seen by analyzing data for several system sizes, not shown here). This is because the modified edge also leads to some amount of y order (middle panel of Fig. 15), and although this induced order decays rapidly when moving away from the modified edge it does not go away completely, even close to the opposite edge.

The rather smooth decay of the y order to almost zero at the opposite edge can be explained as due to the open edge strongly favoring x ordering in its vicinity, even with the modification that breaks the y translational symmetry. The modified edge therefore induces both x and y order, i.e., the VBS angle (22) is $0 < \theta < \pi/2$. Since the second edge does not break the y translational symmetry explicitly, the x ordering can completely dominate there, leading to a very small $\langle D_y\rangle$. The smooth transition from mixed x and y to almost pure x order is seen clearly in the VBS angle graphed in the bottom panel of Fig. 15. Away from the edges, the total order parameter for large systems, $D = (\langle D_x\rangle^2 + \langle D_y\rangle^2)^{1/2}$, approaches the value extracted for this model in the previous section. A maximum in the angle develops with increasing size close to the modified edge.

Figure 16 shows results for systems with the y symmetry broken at both edges. Also in this case it would appear that both the x and y order parameters survive throughout the whole system in the thermodynamic limit. Convergence of both components as well as the angle at the center of the system is seen. The VBS angle here being only slightly less than $\pi/2$ corresponds to an almost equal mixture of x and y order.

In spite of the apparent convergence of the VBS angle to a value close to $\pi/2$ in Fig. 16, the survival of both x and y order in the thermodynamic limit due to the modified edge is illusory. Since the VBS order is columnar, eventually, for very large systems, one would expect only x or only y order to survive. The explanation of the behavior seen is again the very large

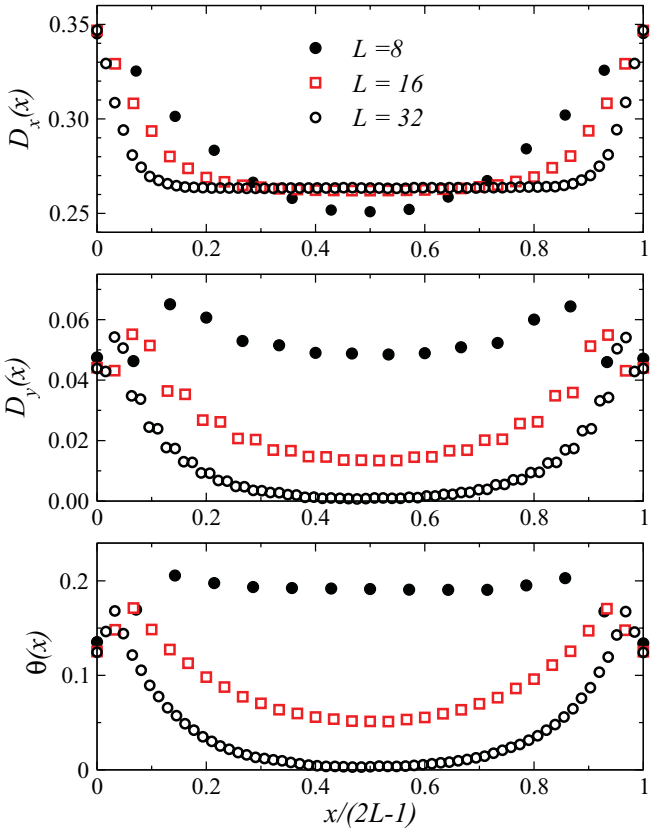

FIG. 17. (Color online) Same as Fig. 16 for the Q_3 model.

U(1)-Z_4 crossover scale in the Q_2 model (as discussed in the Appendix). It is then interesting to look at the same quantities in the Q_3 model, where there is no clear U(1) symmetry (as also shown in the Appendix), i.e., the length scale Λ is very short in this case. Results analogous to those in Fig. 16 for the Q_2 model are shown in Fig. 17 for the Q_3 model. In this case, one can see clearly how the y component vanishes with increasing system size away from the edges, while the x order stabilizes to a constant value. Since the x component is the surviving one, its approach to its bulk value should be governed by the standard VBS correlation length ξ. The decay of the y component should reflect Λ, however (since the presence of y order is due to the angular twisting of the order parameter). This is a direct physical method to access the U(1) length scale, providing an attractive alternative to studying the order-parameter distributions discussed in Appendix.

The decays of the two components are analyzed quantitatively for a larger system in Fig. 18. Excluding the points immediately adjacent to the edge, the decays are of almost pure exponential form (with an even-odd effect seen for the y component), giving $\xi = 1.9$ extracted from the x component and $\Lambda = 6.5$ from the y component. A similar analysis for the Q_2 model (not shown here), based on systems with up to 128×64 sites, gives $\xi \approx 25$ (and Λ much larger still), but this estimate is not reliable because the form of the decay is affected by the proximity to the critical point and is far from a pure exponential at the accessible distances. Larger system sizes are required in this case, especially for extracting Λ, which is larger than 100 lattice constants according to the analysis in the Appendix (perhaps being several hundred lattice constants). A

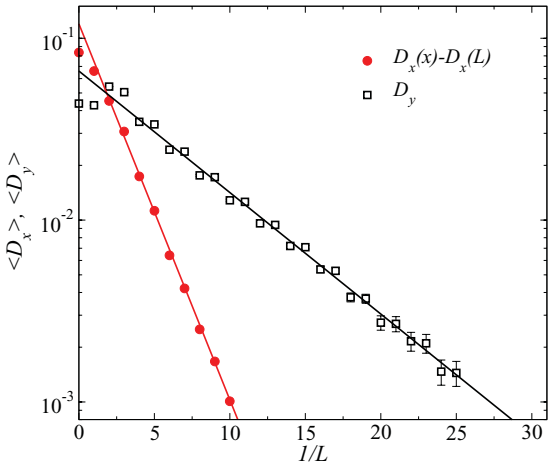

FIG. 18. (Color online) The x and y components of the induced order parameter close to a modified edge of the Q_3 model on a 128×64 lattice. These data are the same as those shown in the top (x) and middle (y) panels of Fig. 17 for smaller systems, but with the nonzero constant behavior at the center of the system subtracted off in the case of the x component. The lines are exponential fits, giving decay lengths 1.9 and 6.5 for the x and y components, respectively.

systematic study of the divergence of the decay lengths of the J-Q_3 model upon approaching the quantum-critical point will be presented elsewhere.

V. LONG CYLINDERS

In the previous sections, the 2D limit was approached in systems with fixed aspect ratio L_x/L_y. In principle, the limit can also be accomplished with one of the lengths taken to infinity first, e.g., $L_x \to \infty$ for fixed L_y and then $L_y \to \infty$. The behavior of the long-distance correlation functions, and, therefore, the squared VBS order parameter $\langle D^2 \rangle$, should not necessarily be expected to be smooth, however. Although VBS ordering amounts to breaking a discrete symmetry, and order can therefore, in principle, exist for any L_y in the infinitely long 1D cylinder geometry, the survival of the order for small L_y is not guaranteed. Clearly, there will be enhanced fluctuations associated with the 1D nature of these systems, which may destroy the ground-state order of a Hamiltonian exhibiting long-range VBS order in the 2D limit.

A well-known system with discrete symmetry breaking is useful for illustrating the potentially unsmooth 1D to 2D crossover: the Ising model with nearest-neighbor coupling J_z in a transverse magnetic field h_x has a phase transition to an ordered (in the z spin direction) state at a critical value $(h_x/J_z)_c$. On a 1D linear chain the critical ratio is $(h_x/J_z)_c = 1$, while on the 2D square lattice it is $(h_x/J_z)_c \approx 3.05$.[97] For an $L_x \times L_y$ lattice with $L_x \to \infty$ one can expect $(h_x/J_z)_c$ to be a monotonic increasing function of L_y. Therefore, for a fixed field $1 < h_x/J_z < 3.05$, one can expect cylinders with small L_y to be disordered, while above some "critical" L_y the system will be ordered. One can expect the same kind of behavior of a 2D VBS as well, when restricting it to a finite cylinder, unless the 2D order parameter is extremely large so that even the smallest cylinder remains in the ordered phase.

In the discussion below, only cylinders of even L_y will be considered, so that the lattice is commensurate with columnar VBS order in both the x and y directions. J-Q models with odd L_y cannot be studied with the QMC method used here, because of sign problems arising due to geometric frustration of the spin interactions.

A. Destruction of VBS order on cylinders

As shown in Sec. III B, the ground state of the pure Q_3 model is strongly VBS ordered, the order parameter being at 70% of the maximum possible value. One might expect this to be sufficient for the order to be stable also on thin cylinders when $L_x \to \infty$. However, it turns out that such cylinders of width $L_y = 4$ and 6 are disordered, while for $L_y = 8$ and above the order parameter is already close to the 2D limiting value. For the pure Q_2 model, where the 2D order parameter is about 20% of the maximum value, no order was found on $L_x \to \infty$ cylinders with L_y up to 12. Larger widths were not studied due to prohibitively long computation times. The results for both models are summarized in Fig. 19. The results underlying these conclusions are discussed next.

It is useful to define correlation functions averaged over the short (y) direction. The following functions, based on the definition (10) of the elementary dimer correlator, can be used to detect columnar VBS order with the bonds oriented either

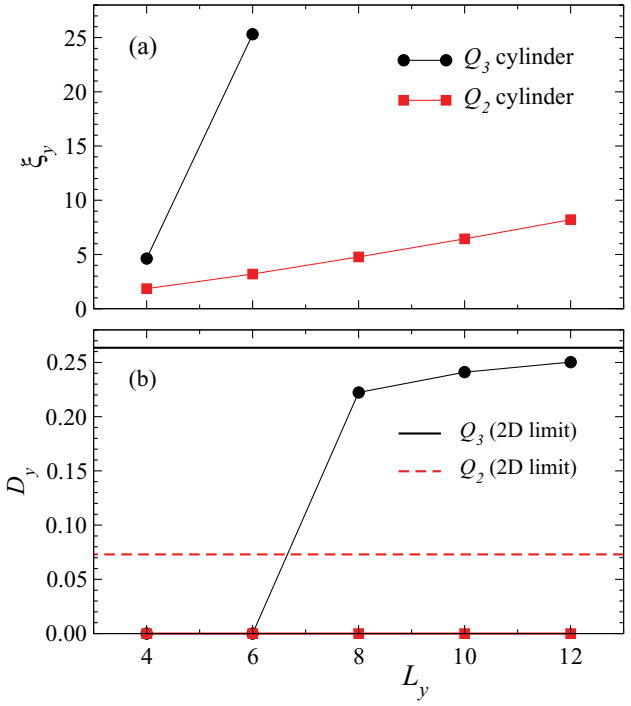

FIG. 19. (Color online) VBS order parameter and correlations lengths on infinite ($L_x \to \infty$) Q_2 and Q_3 cylinders of width $L_y = 4,6,8,10,12$. (a) The correlation length extracted using the dimer correlations with y-oriented bonds as a function of L_y for those cylinders that have disordered ground states (the x correlation lengths are about 5–10% smaller). (b) The order parameter versus L_y, along with the corresponding 2D order parameters (shown with the horizontal lines).

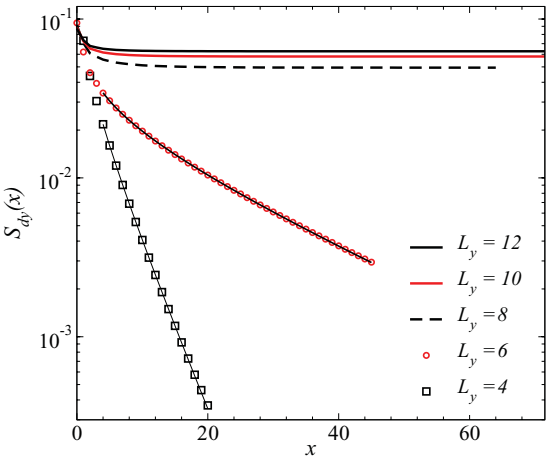

FIG. 20. (Color online) VBS correlation functions, as defined in Eq. (24), for y-oriented dimers in the Q_3 model as a function of the separation in the x direction on cylinders in the $L_x \to \infty$ limit. For $L_y = 4,6$, fitted curves of the form $C \propto \exp(-x/\xi)/x^\alpha$ to the $x \geqslant 4$ data are also shown (with $\alpha \approx 0.5$ in both cases).

along the x or the y direction:

$$S_{dx}(x) = \frac{1}{L_y}\sum_{y=0}^{L_y-1}\left[C_{dx}(x,y) - \frac{1}{2}C_{dx}(x-1,y) - \frac{1}{2}C_{dx}(x+1,y)\right], \quad (23)$$

$$S_{dy}(x) = \frac{1}{L_y}\sum_{y=0}^{L_y-1} C_{dy}(x,y)(-1)^y. \quad (24)$$

Here, it is appropriate to use periodic boundary conditions in both lattice directions. In order to achieve the limit $L_x \to \infty$, aspect ratios L_x/L_y up to 32 were studied for L_y up to 12.

In the Q_3 model, the y-dimer correlator $S_{dy}(x)$ approaches a nonzero constant for large x when $L_y \geqslant 8$, as shown in Fig. 20, while for $L_y = 4,6$ the correlations decays exponentially with distance. The behavior is not purely exponential but follows the form $S_{dy}(x) \propto x^{-\alpha}\exp(-x/\xi)$, with $\alpha \approx 0.5$. This form with $\alpha = 1/2$ is the Ornstein-Zernike (mean-field) form expected in a $d = (1+1)$ dimensional system, where $\alpha = (d-1)/2$. The correlation lengths extracted from fits to this form (with α regarded as a free parameter, to produce somewhat better fits) are shown in Fig. 19(a). The x-oriented correlation function $S_{dx}(x)$ is exponentially decaying for all L_y, i.e., these systems are purely y ordered in the thermodynamic limit (as was also found in Sec. III B for periodic $2L \times L$ systems when $L \to \infty$). For $L_y = 4,6$ the x correlation lengths are slightly smaller than the y ones. The y correlation lengths are graphed in Fig. 19(a).

In Fig. 21, both the x and y correlation functions for the Q_2 model are graphed for all even-width cylinders with $L_y = 4,\ldots,12$, along with fits to the exponential form discussed above. The y correlation length ξ_y is the larger one (about 5–10% larger than ξ_x) and is graphed versus L_y in Fig. 19(a). The correlation length grows roughly linearly with L_y for these cylinders. It would be interesting to go to even larger L_y to study the form in greater detail, and, of course, to find the threshold width for ordering in this case (where presumably

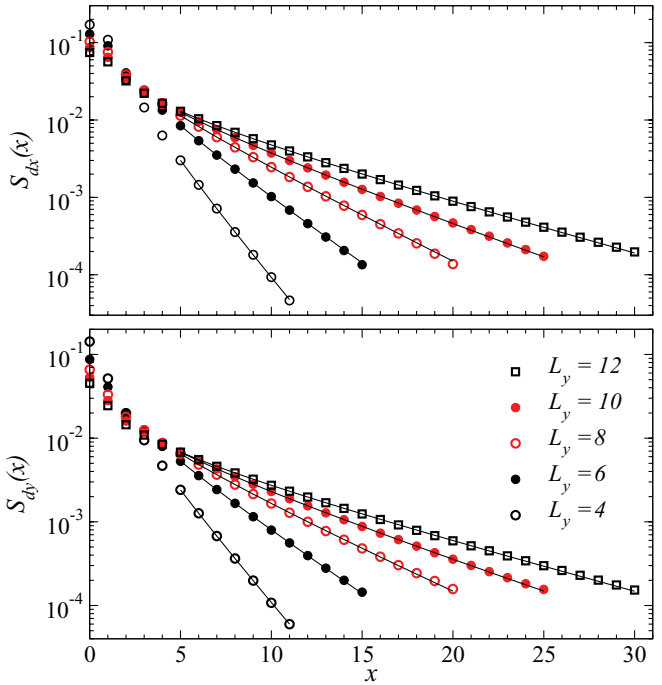

FIG. 21. (Color online) VBS correlation functions, as defined in Eqs. (23) and (24), for x- (top panel) and y-oriented (bottom panel) dimers in the Q_2 model as a function of the separation in the x direction on cylinders in the $L_x \to \infty$ limit. Fits of the data for $x > 4$ to the form $S \propto \exp(-x/\xi)/x^{\alpha}$ (with $\alpha \approx 0.5$ in all cases) are shown as solid curves.

the correlation length should diverge, if one regards L_y as a continuous parameter). The rather small correlation lengths for L_y up to 12 suggest that it may be difficult to reach the critical width with QMC calculations at present.

The destruction of the VBS order even on rather wide cylinders is surprising. In the Q_3 model, judging by the decay of the x component of the order parameter in Fig. 18, the 2D correlation length is approximately two lattice constants. The lower width $L_y = 8$ for ordering on infinitely long cylinders is therefore roughly four times the correlation length. Moreover, related to the short correlation length, the 2D order parameter is as large as 70% of the classical value. One might have expected such a system to be describable essentially in terms of classical (orthogonal, hard-core) dimers with quantum fluctuations of the nature present in quantum dimer models. It has been expected that a VBS under these conditions should be ordered even on narrow cylinders.[52] The results obtained here suggest that the nonorthogonality of the singlets (the true quantum dimers) has a dramatic effects of reducing the order on cylinders, in contrast to this effect actually enhancing the dimmer-dimer correlations relative to those in corresponding dimer models in critical 2D systems.[49,50] On the other hand, to the author's knowledge, quantum dimer models that order in the 2D limit[94] have actually not been extensively studied in long-cylinder geometry. Such studies would clearly be worthwhile, in light of the surprising results obtained here.

In the Q_2 model, the correlation length should be in the range $20 \sim 30$ (with, as already discussed above, the large uncertainty being due to the fact that system sizes $L \gg \xi$ are needed to determine ξ accurately), and one can, thus, expect, roughly, $L_y \approx 100$ to be needed before ordering sets in on the cylinders in this case.

One might speculate that the emergent U(1) symmetry could play some role in destroying the VBS order on the long cylinders. The local coarse-grained VBS order parameter (D_x, D_y) is an essentially isotropic 2D vector up to a large length scale $\Lambda \sim \xi^{1+a}$ with $a > 0$ (with the best estimate so far[40] being $a = 0.20 \pm 0.05$). If the order parameter were truly a vector with isotropic angular fluctuations, long-range order on the 1D $L_x \to \infty$ cylinders would be strictly prohibited.[86] The almost continuous order parameter could then be argued to contribute to the loss of order. If so, one would expect a critical state to replace long-range order, however, of which there are no signs here—the VBS order decaying exponentially starting from short distances. There is no crossover from a critical behavior, which might have been expected if almost U(1) symmetric angular VBS fluctuations were responsible for the destruction of long-range order. The role of emergent U(1) symmetry on cylinders is nevertheless interesting and should be studied more systematically in the future.

Regardless of the exact relationship between the 2D correlation length and the ordering threshold on cylinders, the very short correlation lengths found in the Q_2 model (ranging from about $\xi \approx 2$ for $L_y = 4$ to $\xi \approx 8$ for $L_y = 12$) show the dangers of using the long-cylinder geometry for drawing conclusions about the presence or absence of VBS order in the 2D limit. Order likely appears in the Q_2 model, and probably in most models for which the existence of VBS order

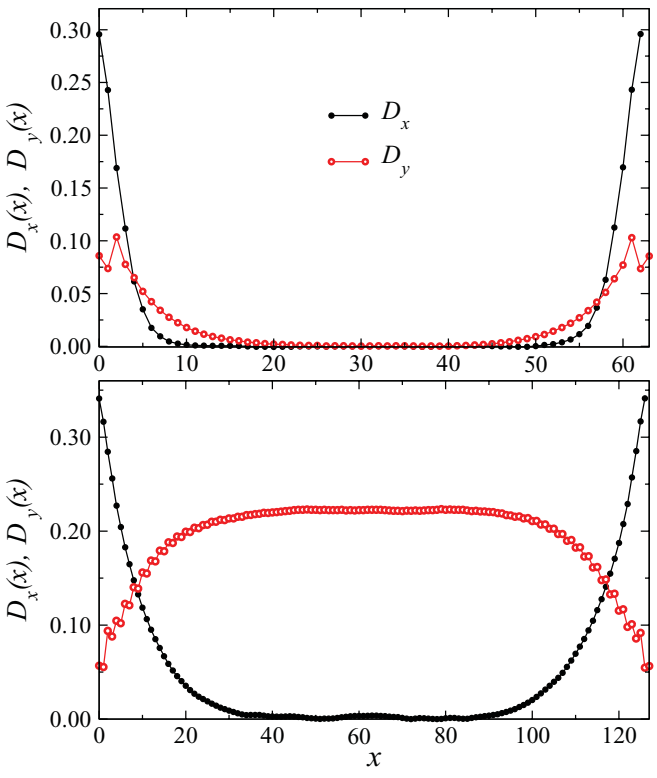

FIG. 22. (Color online) Boundary induced x and y components of the dimer parameter of the Q_3 model on 64×4 (top) and 128×8 (bottom) lattices. Both edges are modified to induce y order, as discussed in Sec. IV.

is under debate, for L_y far exceeding the maximum size that can currently be studied (especially if QMC methods cannot be used and DMRG would be the best choice of method).

The above conclusions regarding ordered and disordered cylinders reached based on correlation functions in long periodic $L_x \times L_y$ systems can also be confirmed by examining open-edge cylinders, in which a unique VBS can be locked in for even L_x (as discussed in the case of $2L \times L$ cylinders in the preceding sections). Figure 22 shows results for longer Q_3 cylinders in which the boundary perturbation inducing y order was also applied at both edges (as in Fig. 14). For $L_y = 4$, both order parameter components decay quickly away from the edges, while for $L_y = 8$, the y component stabilizes at the center of the system, at a value agreeing with that extracted on the basis of the correlation functions [shown in Fig. 19(a)]. Here, although the open edges favor x order more than the perturbations favor y order, the y component eventually wins because that is the component favored just by having a finite L_y, and this effect scales with L_x. In contrast, for the $2L \times L$ cylinders with the same types of edges, it is the x component that survives in the thermodynamic limit, as seen in Fig. 17.

VI. CONCLUSIONS AND DISCUSSION

A. General summary and conclusions

Several benchmark results for the finite-size behavior of the VBS order parameter have been presented in this paper. The J-Q and pure Q models allowed investigations of both strongly and weakly ordered ground states. The main general conclusion (which should be valid for VBS states in many systems) drawn from these studies is that even when the VBS order is relatively strong on the infinite 2D lattice (e.g., 10–20% of the maximum value attainable), results for small and moderate lattices (e.g., with up to hundreds of spins) can exhibit nearly critical behavior. The squared VBS order parameter then appears to extrapolate to zero in the thermodynamic limit. In the J-Q model, this behavior can be traced to a rather large quantum-critical scaling regime around the critical value of J/Q, where the behavior follows closely that obtaining at a critical point.

The extrapolation to infinite size may at first sight seem easier when symmetry-breaking boundaries are used (as is often done in the context of DMRG studies),[2] so that the order parameter can be computed directly (having a considerably larger value than its square when the VBS order is not very strong). However, a small order parameter (10–20% of the maximum value in the VBS systems considered here) is very difficult to extrapolate accurately in this way, partially because the symmetry is not completely broken on lattices of size that can be studied in practice. In particular, the emergent U(1) symmetry of the VBS order parameter implies that the component not locked by the boundaries can survive in the form of significant fluctuations up to very large system sizes, but this aspect of the ordering may be completely missed if one only examines the boundary-induced component of the order parameter. While this effect by itself would probably not lead to wrong conclusions regarding the presence or absence of VBS order, it is still important for explaining results that would otherwise seem inconsistent with each other (e.g., when comparing the total squared order parameter and a direct boundary induced order parameter, as was done here in Sec. III C). The results presented here suggest that the best quantity for extrapolating the order parameter to infinite system size is the total (sum of the x and y components) long-distance correlation functions on $L \times L$ periodic lattices. Nonsquare lattices can lead to nonmonotonic finite-size behavior.

Some of the small-system behaviors pointed out here are generically well known and not limited to VBS order. There are also many examples of finite-size scaling of results for small lattices leading to wrong conclusions of the nature of the ground state. For example, in Refs. 98 and 99, a spin-liquid ground state was claimed to exist in a 2D system of weakly coupled $S = 1/2$ Heisenberg chains. When QMC results for larger systems became available,[69] they showed a crossover of the scaling and an asymptotic behavior in accord with a Néel state for any value of the interchain coupling.

The additional complications due to emergent U(1) symmetry[1,37,38] are more specific to VBS ordering. Open edges twist the vector order parameter (D_x, D_y) in ways which depends on the model and the nature of the edge. For a VBS, there is no "neutral" edge: any boundary affects the ordering pattern in its neighborhood. While in the bulk VBS, in the thermodynamic limit, only one of the components can survive in a columnar state, at edges they can both be present. Due to the large length scale of the crossover from the U(1) symmetric order parameter, both components can also survive in the interior of large systems. It would be interesting to study this phenomenon also in systems with a more complicated (larger unit cell) VBS order parameter.

It should be noted that, although the concept of emergent U(1) symmetry of VBSs was developed in the context of deconfined quantum-critical points and has been confirmed in the case of J-Q models,[1,4,40] this aspect of VBS order is most likely very general and manifested also in systems that are not very close to such critical points (in some extended parameter space)—in 2D systems in which "angular" VBS fluctuations are possible once the correlation length is several lattice constants or larger. The U(1) related boundary effects should be absent in cases where the angular fluctuations are absent, e.g., in the case of staggered VBS states.[75,100]

For the purpose of detecting VBS order, an important aspect of the critical scaling is that, once a critical point has been identified, upward deviations from the power-law behavior, as seen in Fig. 13 at $J/Q_2 = 0$ and 0.03 in the J-Q_2 model, demonstrate an ordered state although this may not be apparent when carrying out extrapolations of the order parameter in $1/L$ (as in Fig. 7). In general, in a model with some tunable parameter that can bring it into or out of a VBS state, it may be easier to detect a phase transition than to extract the exact value of the order parameter close to such a point. On the one hand, many frustrated systems may have VBS states that are always only weakly ordered and, hence, close to a quantum critical point (or weakly first-order transition) in some extended parameter space. Such systems should exhibit near-critical scaling on small lattices. On the other hand, if no critical scaling can be detected, and instead the order parameter correlation function decays exponentially fast with distance (or shows a tendency to decay faster than a power law), one can

rather safely conclude that there is no VBS long-range order. Also with this approach, one can of course not expect to draw reliable conclusions unless the system sizes are sufficiently large (and how large that is depends on the model).

A striking behavior that may be particularly prominent in the case of VBS order was found here for lattices in the form of long cylinders, of size $L_x \times L_y$ with $L_x \to \infty$ and finite even L_y. In this geometry, the order is unstable, and the system exhibits only short-range VBS correlations, until L_y exceeds some threshold that can be very large (perhaps 3–4 times the VBS correlation length, according to results for the Q_3 model). Long cylinders are therefore not ideally suited for determining the nature of the 2D state in which VBS order is a possibility (systems with a small fixed L_x/L_y normally being better). In particular, the method of positively confirming a Z_2 spin liquid by the absence of order on even-L_y systems is not applicable in the "yes-no" sense proposed in Ref. 52. Instead, the finite-size behavior has to be tracked as in any other extrapolation method. The correlation length as a function of even L_y should converge for a spin liquid and diverge for a VBS, as in Fig. 19, but it may not be easy in practice to determine which of these behaviors applies.

B. Comment on the possibility of a spin-liquid state in the J_1-J_2 Heisenberg model

One motivation for the present study was to provide guidance on detecting VBS order—or, alternatively, showing the absence of such order—in calculations for frustrated 2D models. The lattice sizes reachable for such systems with unbiased calculations, primarily using the DMRG method,[3,5,6] are still very limited. Methods based on tensor-product states,[26,30,34] beyond matrix-product states (which are closely related to the DMRG scheme), are still typically too much affected by various truncation errors and approximations to be considered completely unbiased. The following discussion will therefore be primarily aimed at DMRG calculations, although many of the issues would apply more generally.

The issues raised here have particular relevance in the context of a recent DMRG study of the J_1-J_2 Heisenberg model on the square lattice.[4,6] Several different ways of analyzing VBS correlations were argued to consistently show the absence of VBS order and positively confirm the properties of a Z_2 spin liquid. However, many of the results presented can also be explained by a VBS state, at least in some part of the nonmagnetic phase, according to the results obtained here. The key points supporting this view are summarized next.

In Fig. 3 of Ref. 6, second-order polynomial fits to the VBS order parameter for $2L \times L$ cylinders with $L \leqslant 10$ are shown. The fact that these fits extrapolate to negative values in the thermodynamic limit was taken as evidence for the absence of VBS order. However, this kind of behavior is also observed for the Q_2 model on small lattices, as seen in Figs. 7 and 9 of the present paper, even though the order parameter of this model is as large as 20% of the maximum possible value. If VBS order exists also in the nonmagnetic phase of the J_1-J_2 Heisenberg model, one should not expect it to be very strong. Therefore, the finite-size behavior seen in Fig. 3 of Ref. 6 is at least qualitatively what would be expected even if the state is a VBS. It should be noted that the fact that the fitted functions extrapolate to negative values is in itself a clear sign of the chosen functional forms not being correct, as the squared order parameter cannot be negative. Thus there must necessarily be a crossover to a different form for larger systems—either to a pure $1/L^2$ form, if there is no long-range order, or to an exponentially rapidly convergent form tending to a nonzero value. The results for small systems cannot distinguish between these different asymptotics.

The finite-size extrapolation issues may clearly also affect the determination of the transition point between the Néel antiferromagnet and the nonmagnetic state at $g = J_2/J_1 \approx 0.4$ (while the transition point into the stripe antiferromagnet at $g = J_2/J_1 \approx 0.6$ is much easier to extract due to it being clearly first order). The transition point $g \approx 0.41$ was determined in Ref. 6 based on extrapolations of the Néel order parameter $\langle M^2 \rangle$ using second-order polynomials, and these should be affected by similar problems as those pointed out here for the VBS scaling (and it is also well known that polynomials higher than second order have to be used to extrapolate Néel order correctly based on small systems, even in the strongly order Heisenberg model).[69,80] The Néel order should therefore survive up to somewhat larger g values. Thus, at $g = 1/2$, on which most of the analysis of the VBS scaling was focused in Ref. 6, the system may be rather close to the transition point. If VBS order exists in the nonmagnetic phase, it would therefore likely be very weak at this point. In Fig. 3(a) of Ref. 6, the maximal value of the order parameter $\langle D_y^2 \rangle$, at g just below 0.6, is close to the values for the Q_2 model in Fig. 9 of the present paper. Thus if the J_1-J_2 model has VBS order, its peak value should be about 10–20% of that of a perfect columnar state. It would be better to analyze the VBS correlations closer to the maximal value, where the extrapolation problems are minimized.

As discussed in Sec. III D, in systems where there is a quantum phase transition into the state of interest, the best way to deduce the nature of that state may be to first carefully examine the phase transition. If there is critical scaling, deviations from the power-law form of the order parameter away from the critical point can be a good signal of long-range order. However, as seen in the scaling plot for the near-critical J-Q_2 model in Fig. 13, if the accessible system sizes are only up to $L \approx 10$, even a system in which the VBS order parameter is as large as 20% of the maximum value may in practice not be distinguishable from a critical system when analyzing the order parameter fluctuations. If the nonmagnetic state of the J_1-J_2 Heisenberg model also has long range order, then one should expect a similar behavior.

Replotting the $g = 0.5$ and 0.56 data for the VBS y component of Fig. 3(a) of Ref. 6 on a log-log scale, one can indeed observe behaviors close to power laws, as shown in Fig. 23(a). In the same graph data for the J-Q_2 model at $J = 0$ and $J_c = 0.0447$ are also graphed. In this case, the x component of the order parameter is shown, which, as seen in Fig. 9, in this system is larger than the y component and is the one surviving in the thermodynamic limit. In the J_1-J_2 model, it is instead the x component that is somewhat larger.[101]

The comparison of the two models is complicated by the fact that the average induced x order was subtracted in the definition used in Ref. 6. That induced order is very small, however,[101] unlike what it is in the Q_2 model (which, may

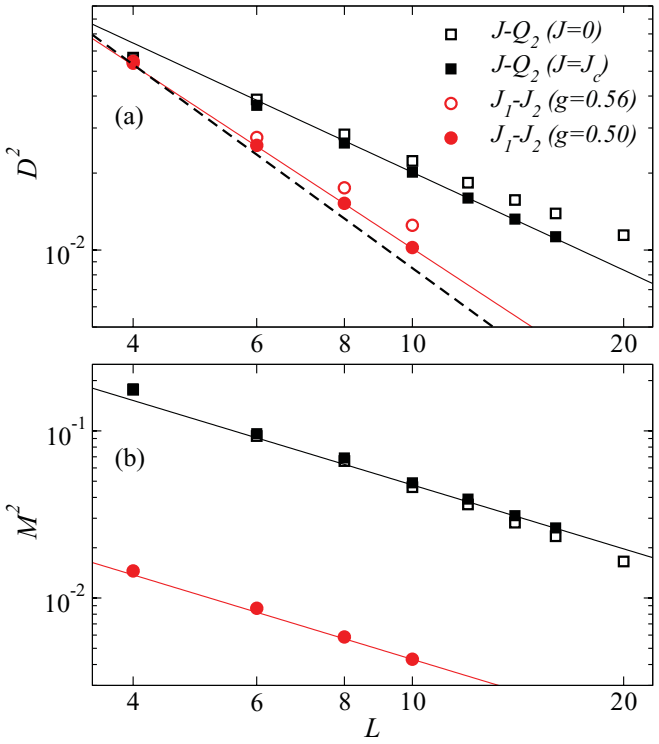

FIG. 23. (Color online) Finite-size scaling of the squared VBS order parameter (a) and staggered magnetization (b) calculated on the central $L \times L$ square of cylinders of size $2L \times L$. DMRG results for the J_1-J_2 model at $g = 0.50$ and 0.56, from Figs. 2(a) and 3(a) of Ref. 6, are compared with QMC results for the J-Q_2 model at its critical point, $(J/Q_2)_c = 0.0447$, and at $J = 0$. In (a), the VBS y component of the J_1-J_2 model and the x component (the larger component) of the J-Q_2 are shown. The line drawn close to the $J/Q_2 = 0.0447$ points has slope -1.27, corresponding to the critical exponent $\eta = 0.27$ (as in Fig. 13), and that going through the $g = 0.50$ points has slope -1.8. The dashed line has slope -2, corresponding to the expected asymptotic behavior in a non-VBS state. In (b), both lines have slope -1.27 ($\eta = 0.27$).

indicate that the VBS order, if it exists in the J_1-J_2 model, is y oriented on the cylindrical $2L \times L$ systems, as was also noted in Ref. 6).

For the open-edge $2L \times L$ cylinders used in Fig. 23(a), the J-Q_2 results do not exhibit quite as good scaling as in the case of the periodic $L \times L$ systems in Fig. 13, but for large systems the behavior is still consistent with an exponent $\eta \approx 0.3$. The J_1-J_2 results for $g = 0.5$ follow a different behavior, however, decaying as $L^{-\alpha}$ with $\alpha \approx 1.8$. This is quite close to $\alpha = 2$, which is expected deep inside a non-VBS phase. For $g = 0.56$, the data for the larger sizes deviate significantly upward from the $g = 0.5$ points and cannot be fitted very well to a power law. The slope on the log-log scale is ≈ -1.52 for a line drawn through the $L = 8$ and 10 points, but the data for smaller systems fall above the fitted line, showing a flattening out with increasing size. The reduction of the rate of decay is opposite to the expectation for a spin liquid and an indication that the system is VBS ordered in the infinite-size limit.

The behavior at $g = 0.5$ is puzzling. Since the VBS order parameter here follows quite close to the form expected in a spin liquid, one may conclude that this is what it is, and the deviations from the $\sim 1/L^2$ form are due to remaining size effects (i.e., the system size is not yet much larger than the correlation length). A possibility suggested by the behavior observed in Fig. 23 is that the J_1-J_2 model has a spin-liquid phase following the Néel phase above $g \approx 0.4$, followed in turn by a VBS at larger g (since the $g = 0.56$ results seem more indicative of weak VBS order). Another possibility is that there is no spin liquid, but the Néel-VBS transition takes place at g significantly larger than previously believed, so that $g = 0.5$ would actually still be inside the Néel phase. Looking at the raw data for the sublattice magnetization in Fig. 2(a) of Ref. 6, it appears that this possibility cannot be ruled out (considering again also the fact that the second-order polynomial fits used should lead to an under-estimation of the critical g where the Néel order vanishes). The behavior of the triplet gap in Fig. 2(b) seems to go against this scenario, however, although the way the gap was extracted, by targeting higher states obtained while keeping the edges in the ground state, may lead to strong corrections to the gap scaling.

To investigate possible near-criticality in the Néel order parameter, the results from Fig. 2(a) of Ref. 6 for $\langle M^2 \rangle$ at $g = 0.5$ are replotted on a log-log scale in Fig. 23(b). Interestingly, the behavior follows closely a power law, with an exponent η very similar to that of the J-Q_2 model. This could indicate that the transition out of the Néel state indeed takes place close to $g = 0.5$ and is in the same universality class as the J-Q model. Note that, within the deconfined quantum criticality theory,[37] this kind of criticality of the magnetic order would not necessarily require that the VBS order emerges at this point as well, because the exponents associated with the Néel order parameter are not affected by the VBS (since the operator causing the VBS order is dangerously invariant). Clearly, there is not sufficient data here to make any firm conclusions about this scenario of a Néel to spin-liquid transition, possibly followed by a subsequent liquid to VBS transition at higher g, but the behavior is intriguing and deserves further tests.

An important aspect of the analysis of Ref. 6, cited as positive evidence for a Z_2 spin liquid, is the behavior of the order parameter on infinitely long cylinders. There is an even-odd effect that had previously been found in liquid states of quantum dimer models:[52] For odd L_y and even $L_x \to \infty$, an x-oriented order parameter $\propto \exp(-L_y/\xi_y)$ is induced because of geometric frustration effects. For even L_y, no order is observed at all, regardless of the type of VBS (horizontal or vertical columns) favored by the edges. Unfortunately, odd-L_y J-Q cylinders cannot be studied with the QMC method used here, because of sign problems. However, based on the results presented here for even L_y it is already clear that this kind of test for a Z_2 spin liquid may not be that useful in practice, because VBS order does not exist on the infinitely long cylinders (for L_y up to some critical width that can be expected to be inaccessible in practice for systems that are weakly to moderately ordered in the 2D limit). In Ref. 6, it was implicitly assumed that any system with 2D VBS order will exhibit such order also on long thin cylinders.

It is also interesting to note that the induced order parameter as a function of the distance from a modified edge of systems in the $L_x \to \infty$ limit is very similar in the J_1-J_2 and J-Q_2

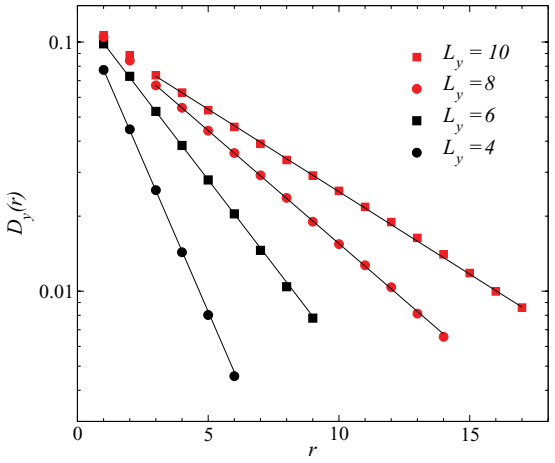

FIG. 24. (Color online) VBS y order parameter component induced by edges modified to break the y translational symmetry (as explained in Fig. 14) in the Q_2 model. Here, r is defined as the distance from the second column of spins away from the edge, since the edge modification extends to this location. The lines show exponential fits, with decay lengths 1.8 ($L_y = 4$), 3.2 ($L_y = 6$), 4.8 ($L_y = 8$), and 6.6 ($L_y = 10$).

models. Figure 24 shows results for the pure Q_2 model on cylinders of width 4–10 in which the edge has been modified to break the y translational symmetry, as discussed in Sec. IV and illustrated in Fig. 14. Here, cylinders with aspect ratio $L_x/L_y = 16$ were used (which is large enough to accurately represent the $L_x \to \infty$ limit). The edge-induced x and y order parameters both decay exponentially, with very similar decay lengths that are also close to the correlation lengths graphed in Fig. 19 (obtained from correlation functions on systems with all periodic boundaries). The y decay lengths are always marginally larger. For $L = 6$ and 8, the decay lengths are about 1.5 times those in the J_1-J_2 model at $g = 0.5$, for which data were shown in Fig. S6(b) of Ref. 6.

As discussed above and seen clearly in Fig. 23, the VBS order parameter is likely significantly suppressed at $g = 0.5$ relative to what it is close to its maximum in this model (which appears to be a bit above 0.56). One can therefore expect to see decay lengths as large as those in the Q_2 model for larger g (close to 0.6). The rapid decay was in Ref. 6 interpreted as the system being insusceptible to VBS ordering even in the presence of, at first sight, very favorable conditions for inducing it. Again, when analyzed in light of the known physics of the J-Q_2 model, the results cannot be distinguished from those of a rather substantially ordered VBS. It would be illuminating to have J_1-J_2 data for $L_y > 8$, to see if the decay length continues to grow or saturates.

In Ref. 6, the size dependence of the entanglement entropy was also used as positive evidence of a Z_2 spin liquid. It would be very interesting to compute this quantity also for the J-Q models. It is clear that the nontrivial aspects of the VBS fluctuations could lead to behaviors not predicted in the strong-VBS limit. Since the system on small lattices and cylinders resembles a spin liquid, it would not be surprising if the corrections to the area law of the entanglement entropy are also similar, up to some large size where the true asymptotic VBS behavior sets in. QMC calculations of the entanglement entropy of the J-Q models will be carried out in future studies, using the recent developments of methods to study the Renyi versions of the entropies.[102,103] This should clarify whether the constant deviation from the area law cited in Ref. 6 is really unique to Z_2 spin liquids, or whether they can also appear (for lattices of practically reachable size) in weakly ordered VBS states. The scaling of the entanglement entropy at a deconfined quantum-critical point is also of interest here.[104]

The conclusion reached from the above comparisons of results for the J_1-J_2 model and the J-Q models is that they exhibit rather similar behaviors, and, therefore, a VBS ground state of the J_1-J_2 cannot be excluded. Some of the J_1-J_2 results may also be consistent with a Z_2 spin liquid at $g \approx 0.5$, but the point to note here is that most of the results presented so far do not favor that kind of state over a VBS state. In particular, the claimed positive signals for a Z_2 spin liquid are also seen in the confirmed VBS state of the J-Q models. If anything, the very similar behaviors seen in the near-critical Q_2 model and the J_1-J_2 models should tilt the balance further in favor of VBS order for $g = J_2/J_1$ close to 0.6. The behavior at $g = 0.5$ is very intriguing and not consistent with a near-critical VBS of the same kind as in the J-Q models. It would be very useful to analyze the VBS and magnetic correlations further in this case, preferrably on larger lattices.

It would also be good to know in greater detail the effects of truncation (the number of states kept) in the DMRG calculations. The error $\approx 10^{-7}$ in Ref. 6 refers to the missing weight in the density matrix. One can expect the errors in the wave function to be approximately the square-root of this error,[3,66] but exactly how much the VBS correlations are affected, especially for the largest systems, is not entirely clear.

C. Remarks on other potential spin liquids

The results presented here also are relevant to studies of the kagome Heisenberg model, for which DMRG studies also have indicated a spin-liquid state.[4,5] A VBS is another candidate state,[33,34] which is not easy to exclude if the ordering is weak (which should be expected, if this kind of order is present). Since the most likely VBS patterns in this case are much more complicated than the columnar state of the J-Q models discussed here (with the most likely candidate states having 12- or 36-spin unit cells), it is not possible to relate results in the same close manner as done above in the case of the J_1-J_2 model. Nevertheless, the issues pointed out here should be considered also when analyzing the kagome system, in particular on long cylinders. It would be very desirable to reach larger $L_x \times L_y$ lattices with the aspect ratio L_x/L_y kept fixed, although this seems difficult at present. It would also be good to push calculations based on the multiscale entanglement renormalization ansatz (MERA)[34] to higher precision. Such a calculation had previously seemed to confirm the VBS with 36-site cell proposed earlier based on other techniques,[31,33] but the energy reached was not as low as that found with DMRG[4,5] and exact diagonalization.[64,65]

The analysis and arguments presented in this paper also suggest that it would be very useful to add to the nearest-neighbor Heisenberg exchange some term that favors one of the VBS states proposed previously, and to study the phase transition out of this ordered state. Longer-range couplings

may work, but some interaction similar to the multispin Q terms discussed here could be even better suited for inducing the desired type of VBS.

Spin liquid states have recently also been claimed to exist in electronic Hubbard models and frustrated spin models on the honeycomb lattice.[105–107] For the Hubbard model, 2D lattices with up to hundreds of sites were used.[105] The VBS correlations in this case decay very rapidly with distance, and the system does not seem to exhibit the kind of problematic scaling issues pointed out in this paper. On the other hand, work on effective spin models constructed to capture the putative spin-liquid state have not so far been conclusive.[62,107–109] Also here it would be useful to extend the models in such a way that a VBS phase transition can be studied. The VBS should then be the one to which the "bare" honeycomb model is the most susceptible (which may in itself not be easy to determine in this case).

D. Bench-mark challenge

Finally, as a challenge to DMRG, tensor-product, and MERA techniques, it would be very interesting and useful to see these methods applied to J-Q models as well. Comparing with the known phase diagram and critical behavior extracted on the basis of unbiased QMC simulations would be a very good test of the capabilities of these methods to capture nontrivial ground states and quantum phase transitions. If the outcome is positive, it may be very useful to systematically investigate the behavior when frustration is added to this model, as was recently done in an exact diagonalization study of a 2D model combining the Q_2 interaction with the frustrated J_1-J_2 Heisenberg model.[110]

ACKNOWLEDGMENTS

I would like to thank Leon Balents, Ying-Jer Kao, Roger Melko, Rajiv Sing, Ying Tang, and Steve White for stimulating discussions and comments on the manuscript. I am also indebted to all the authors of Ref. 6 for providing numerical data from their manuscript and for discussing additional unpublished results. This research was supported by the NSF under Grant No. DMR-1104708. Part of the work was carried out during a visit to National Taiwan University. I would like to thank its Center for Advanced Study in Theoretical Science for hospitality and support from Grant No. NTU 10R80909-4.

APPENDIX: U(1)-Z_4 CROSSOVER OF THE VBS SYMMETRY IN PERIODIC SYSTEMS

The emergent U(1) symmetry of a columnar VBS in the neighborhood of a critical point can be characterized by the probability distribution $P(D_x,D_y)$ generated in QMC simulations on periodic $L \times L$ lattices. A systematic study aimed at extracting the scaling of the U(1)-Z_4 crossover length Λ was presented in Ref. 40. Here, additional results for the pure Q_2 and Q_3 models will be presented in order to facilitate comparisons with the boundary effects discussed in the main text. Specifically, it will be shown that the lack of D_x-D_y symmetry on $2L \times L$ lattices, as seen in Fig. 4 for the Q_3 model for all system sizes, is matched by a clear Z_4 symmetric order parameter on all $L \times L$ lattices. Conversely, the symmetry seen for the Q_2 model on large lattices in Fig. 4 is consistent with only very small deviations (barely detectable) from U(1) symmetry on $L \times L$ lattices with L as large as 128.

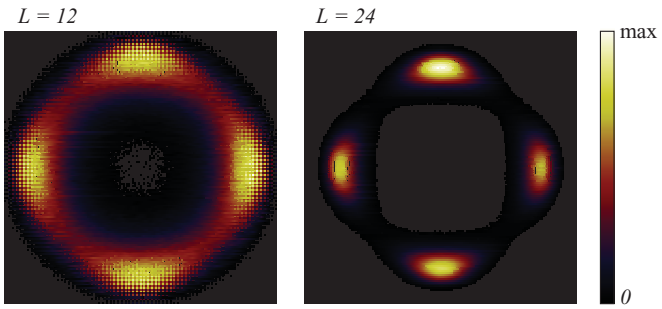

FIG. 25. (Color online) VBS order parameter distribution $P(D_x,D_y)$ in the Q_3 model on periodic $L \times L$ lattices with $L = 12$ (left) and $L = 24$ (right). The size of both squares corresponds to the full space of possible values of the components $D_x,D_y \in [-D_{\max},D_{\max}]$, where $D_{\max} = 3/8$ (for a perfect columnar VBS).

In the projector QMC simulations, each generated configuration is associated with a pair of order parameters (D_x,D_y), which are matrix elements of the corresponding operators defined in Eqs. (12) and (13) computed in the valence bond basis. These matrix elements are of the form $3n/4N$, where n is an integer in the range $[-N/2,N/2]$, with the extremal values corresponding to both the bra and ket state (making up the transition graph) having the same perfect columnar pattern of valence bonds of length one lattice constant. The histogram $P(D_x,D_y)$ is constructed based on these matrix elements.

Figure 25 shows results for the Q_3 model for $L = 12$ and 24. In this model, the histogram $P(D_x,D_y)$ exhibits a distinct fourfold symmetry even for the smallest systems (also smaller than $L = 12$, not shown here, where the discreteness of the distribution function also becomes apparent). The four peaks sharpen with increasing lattice size, and above some size the suppression of the weight between the peaks severely impedes QMC fluctuations between the peaks. In Fig. 25, the visibly different weight in the four peaks (with the right peak having the smallest weight) is a consequence of this rarity of

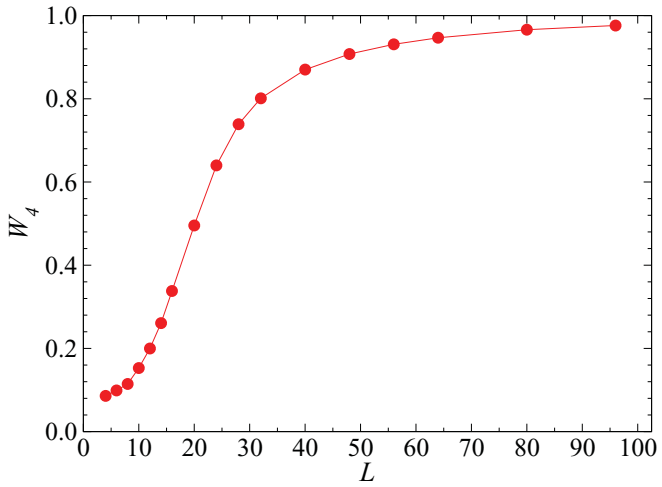

FIG. 26. (Color online) Size dependence of the columnar anisotropy weight, defined in Eq. (A1), of the VBS order parameter distribution in the Q_3 model.

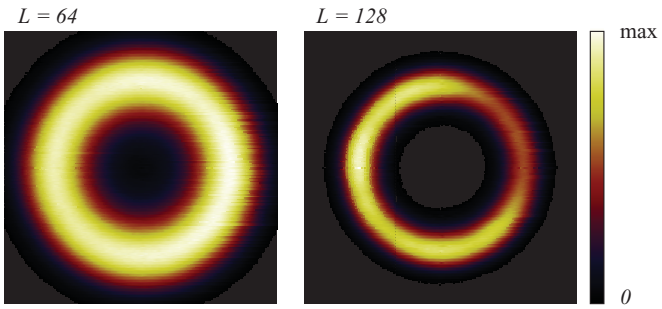

FIG. 27. (Color online) VBS order parameter distribution $P(D_x, D_y)$ in the Q_2 model on periodic $L \times L$ lattices with $L = 64$ (left) and $L = 128$ (right). The size of both squares corresponds to 10% of the maximum value $D_{\max}/10$ of the components, $D_x, D_y \in [-D_{\max}, D_{\max}]$, where $D_{\max} = 3/8$ (for a perfect columnar VBS).

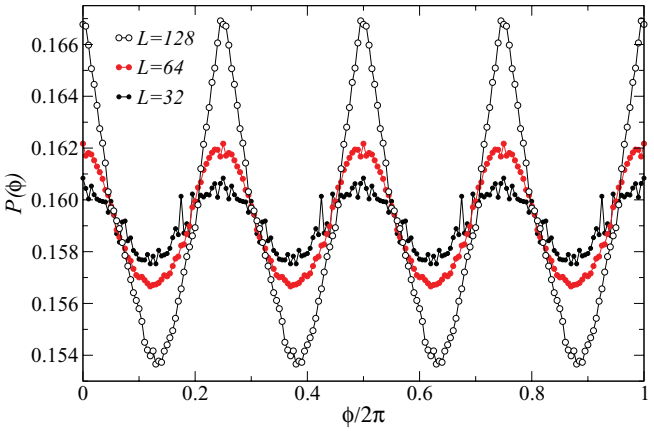

FIG. 28. (Color online) Angular distribution of the VBS order parameter of the Q_2 model for system sizes $L = 32$, 64, and 128. To improve the statistics, these results were obtained by symmetrizing the distributions using the expected 90° rotational symmetry. The jaggedness of the curves (especially for $L = 32$) is due to the discreteness of the allowed (D_x, D_y) values (with N possible values for each component).

"instanton" events between the peaks (i.e., the simulations "get stuck" in one quarter of the configuration space). It should be noted that this very slow simulation dynamics of the VBS order parameter does not affect the estimate of the total squared order parameter $\langle D^2 \rangle$ and most other physical quantities of interest.

The degree of Z_4 symmetry of the order parameter can be quantified by the function

$$W_4 = \sum_{D_x} \sum_{D_y} P(D_x, D_y) \cos(4\phi_{xy}), \qquad \text{(A1)}$$

where ϕ_{xy} is the angle corresponding to the point (D_x, D_y). While this function (and the underlying probability distribution) is not a physical observable, in the sense that it is not a *bona fide* quantum mechanical expectation value, it, nevertheless, reflects the fluctuations of the VBS order parameter and can be used to characterize the the U(1)-Z_4 crossover.

Results as a function of L for the Q_3 model are shown in Fig. 26. Here, the convergence $W_4 \to 1$ when $L \to \infty$ is apparent, as would be expected for a columnar VBS in the thermodynamic limit. In principle, the curve $W_4(L)$ could be used to define the length Λ, e.g., using $W_4(\Lambda) = 1/2$, but there is clearly an arbitrariness in choosing the particular number. For studying the scaling of Λ when some parameter of the Hamiltonian is changed (e.g., J/Q_3) this ambiguity does not matter. In Ref. 40, curves $W_4(L)$ for different coupling rations were analyzed using standard finite-size scaling techniques, with the results that Λ grows slightly faster than the correlation length $\Lambda \sim \xi^{1+a}$ with $a \approx 0.2$.

Comparing with the behavior of the squared order parameters in Fig. 4, it can be noted that $\langle D_x^2 \rangle$ approaches 0 (and $\langle D_y^2 \rangle$ tends to a nonzero value) very quickly above $L \approx 20$, which is approximately where $W_4(L) = 1/2$ in Fig. 26. On the other hand, the decay of the edge-induced y component of the order parameter in Figs. 17 and 18 (where the system far from theedge has only x order) gives a length ≈6.5, which could also be taken as a practical definition of Λ. This length corresponds to $W_4 \approx 0.1$ in Fig. 26.

In contrast to the Q_3 model, in the Q_2 model no clear Z_4 symmetry is visible in $P(D_x, D_y)$ up to systems as large as $L = 64$ and 128, as shown in Fig. 27. These histograms are ring-shaped, although for $L = 128$ the weight is not evenly distributed because of lack of sufficient QMC statistics. The VBS angle fluctuates very slowly in simulations of large systems and very long runs are required in order to obtain symmetric distributions. The data shown are based on $\approx 3.5 \times 10^8$ Monte Carlo sweeps for $L = 64$ and 8×10^7 for $L = 128$ (which required more than 10^4 CPU hours in both cases). By symmetrizing the distributions using 90° rotations, one can still detect small deviations from perfect U(1) symmetry, as shown in Fig. 28. The peak positions again correspond to a columnar state.

Note that in Fig. 27 the ring for $L = 128$ is considerably thinner than for $L = 64$, with the radius (the location of the maximum or average weight) remaining almost unchanged. This reflects an expected reduction of the fluctuations of the magnitude of the VBS order parameter with increasing system size. Based on these results, the crossover length scale Λ for the Q_2 model should be $\gg 128$, which explains why both order-parameter components are essentially equal for the largest systems in Fig. 8.

[1] A. W. Sandvik, Phys. Rev. Lett. **98**, 227202 (2007).
[2] S. R. White and A. L. Chernyshev, Phys. Rev. Lett. **99**, 127004 (2007).
[3] E. M. Stoudenmire and S. R. White, Annu. Rev. Cond. Matt. Phys. **3**, 111 (2012).
[4] H.-C. Jiang, Z. Y. Weng, and D. N. Sheng, Phys. Rev. Lett. **101**, 117203 (2008).
[5] S. Yan, D. A. Huse, and S. R. White, Science **332**, 1173 (2011).
[6] H.-C. Jiang, H. Yao, and L. Balents, e-print arXiv:1112.2241.
[7] C. K. Majumdar and D. K. Ghosh, J. Math. Phys. **10**, 1388 (1969); **10**, 1399 (1969).
[8] K. Nomura and K. Okamoto, Phys. Lett. A **169**, 433 (1992).
[9] S. Eggert, Phys. Rev. B **54**, R9612 (1996).
[10] A. W. Sandvik, AIP Conf. Proc. **1297**, 135 (2010).

[11] I. Affleck, Phys. Rev. Lett. **55**, 1355 (1985).
[12] R. Bursill, G. A. Gehring, D. J. J. Farnell, J. B. Parkinson, T. Xiang, and C. Zeng, J. Phys.: Condens. Matter **7**, 8605 (1995).
[13] M. Kumar, Z. G. Soos, D. Sen, and S. Ramasesha, Phys. Rev. B **81**, 104406 (2010).
[14] P. Chandra and B. Doucot, Phys. Rev. B **38**, 9335 (1988).
[15] E. Dagotto and A. Moreo, Phys. Rev. Lett. **63**, 2148 (1989).
[16] N. Read and S. Sachdev, Phys. Rev. Lett. **62**, 1694 (1989).
[17] R. R. P. Singh and R. Narayanan, Phys. Rev. Lett. **65**, 1072 (1990).
[18] N. Read and S. Sachdev, Phys. Rev. Lett. **66**, 1773 (1991).
[19] H. J. Schulz, T. Ziman, and D. Poilblanc, J. Phys. I **6**, 675 (1996).
[20] V. N. Kotov, J. Oitmaa, O. P. Sushkov, and Z. Weihong, Phys. Rev. B **60**, 14613 (1999).
[21] R. R. P. Singh, Z. Weihong, C. J. Hamer, and J. Oitmaa, Phys. Rev. B **60**, 7278 (1999).
[22] O. P. Sushkov, J. Oitmaa, and Z. Weihong, Phys. Rev. B **63**, 104420 (2001).
[23] L. Capriotti and S. Sorella, Phys. Rev. Lett. **84**, 3173 (2000).
[24] M. Mambrini, A. Läuchli, D. Poilblanc, and F. Mila, Phys. Rev. B **74**, 144422 (2006).
[25] K. S. D. Beach, Phys. Rev. B **79**, 224431 (2009).
[26] V. Murg, F. Verstraete, and J. I. Cirac, Phys. Rev. B **79**, 195119 (2009).
[27] L. Isaev, G. Ortiz, and J. Dukelsky, Phys. Rev. B **79**, 024409 (2009).
[28] X.-G. Wen, Phys. Rev. Lett. **90**, 016803 (2003).
[29] L. Capriotti, F. Becca, A. Parola, and S. Sorella, Phys. Rev. Lett. **87**, 097201 (2001).
[30] L. Wang, Z.-C. Gu, X.-G. Wen, and F. Verstraete, e-print arXiv:1112.3331.
[31] J. B. Marston and C. Zeng, J. Appl. Phys. **69**, 5962 (1991).
[32] P. Nikolic and T. Senthil, Phys. Rev. B **68**, 214415 (2003).
[33] R. R. P. Singh and D. A. Huse, Phys. Rev. B **76**, 180407 (2007); **77**, 144415 (2008).
[34] G. Evenbly and G. Vidal, Phys. Rev. Lett. **104**, 187203 (2010).
[35] D. Poilblanc, M. Mambrini, and D. Schwandt, Phys. Rev. B **81**, 180402(R) (2010).
[36] S. Sachdev, Phys. Rev. B **45**, 12377 (1992).
[37] T. Senthil, A. Vishwanath, L. Balents, S. Sachdev, and M. P. A. Fisher, Science **303**, 1490 (2004).
[38] M. Levin and T. Senthil, Phys. Rev. B **70**, 220403 (2004).
[39] R. G. Melko and R. K. Kaul, Phys. Rev. Lett. **100**, 017203 (2008); R. K. Kaul and R. G. Melko, Phys. Rev. B **78**, 014417 (2008).
[40] J. Lou, A. W. Sandvik, and N. Kawashima, Phys. Rev. B **80**, 180414(R) (2009).
[41] A. W. Sandvik, Phys. Rev. Lett. **104**, 177201 (2010).
[42] A. W. Sandvik, V. N. Kotov, and O. P. Sushkov, Phys. Rev. Lett. **106**, 207203 (2011).
[43] A. Banerjee, K. Damle, and F. Alet, Phys. Rev. B **83**, 235111 (2011).
[44] M. Hermele, T. Senthil, M. P. A. Fisher, P. A. Lee, N. Nagaosa, and X.-G. Wen, Phys. Rev. B **70**, 214437 (2004).
[45] J. Cano and P. Fendley, Phys. Rev. Lett. **105**, 067205 (2010).
[46] P. W. Anderson, Science **235**, 1196 (1987).
[47] B. Sutherland, Phys. Rev. B **37**, 3786 (1988); **38**, 6855 (1988).
[48] S. Liang, B. Doucot, and P. W. Anderson, Phys. Rev. Lett. **61**, 365 (1988).
[49] Y. Tang, A. W. Sandvik, and C. L. Henley, Phys. Rev. B **84**, 174427 (2011).
[50] A. F. Albuquerque and F. Alet, Phys. Rev. B **82**, 180408 (2010).
[51] Y. Iqbal, F. Becca, and D. Poilblanc, Phys. Rev. B **84**, 020407 (2011).
[52] H. Yao and S. A. Kivelson, e-print arXiv:1112.1702.
[53] A. W. Sandvik and R. Moessner, Phys. Rev. B **73**, 144504 (2006).
[54] K. S. Raman, R. Moessner, and S. L. Sondhi, Phys. Rev. B **72**, 064413 (2005).
[55] A. Kitaev, Ann. Phys. (NY) **321**, 2 (2006).
[56] F. Wang, Phys. Rev. B **81**, 184416 (2010).
[57] L. Dang, S. Inglis, and R. G. Melko, Phys. Rev. B **84**, 132409 (2011).
[58] A. Kitaev and J. Preskill, Phys. Rev. Lett. **96**, 110404 (2006).
[59] M. Levin and X.-G. Wen, Phys. Rev. Lett. **96**, 110405 (2006).
[60] P. Henelius and A. W. Sandvik, Phys. Rev. B **62**, 1102 (2000).
[61] M. Nyfeler, F.-J. Jiang, F. Kämpfer, and U.-J. Wiese, Phys. Rev. Lett. **100**, 247206 (2008).
[62] B. K. Clark, D. A. Abanin, and S. L. Sondhi, Phys. Rev. Lett. **107**, 087204 (2011).
[63] J. Richter and J. Schulenburg, Eur. Phys. J. B **73**, 117 (2010).
[64] H. Nakano and T. Sakai, J. Phys. Soc. Jpn. **80**, 053704 (2011).
[65] A. M. Läuchli, J. Sudan, and E. S. Sørensen, Phys. Rev. B **83**, 212401 (2011).
[66] U. Schollwöck, Ann. Phys. (NY) **326**, 96 (2011).
[67] B. Bauer, G. Vidal, and M. Troyer, J. Stat. Mech. (2009) P09006.
[68] H. H. Zhao, Z. Y. Xie, Q. N. Chen, Z. C. Wei, J. W. Cai, and T. Xiang, Phys. Rev. B **81**, 174411 (2010).
[69] A. W. Sandvik, Phys. Rev. Lett. **83**, 3069 (1999).
[70] F.-J. Jiang, Phys. Rev. B **85**, 014414 (2012).
[71] K. H. Höglund and A. W. Sandvik, Phys. Rev. B **79**, 020405(R) (2009).
[72] R. K. Kaul, R. G. Melko, M. A. Metlitski, and S. Sachdev, Phys. Rev. Lett. **101**, 187206 (2008).
[73] A. W. Sandvik, S. Daul, R. R. P. Singh, and D. J. Scalapino, Phys. Rev. Lett. **89**, 247201 (2002).
[74] F.-J. Jiang, M. Nyfeler, S. Chandrasekharan, and U.-J. Wiese, J. Stat. Mech. (2008) P02009.
[75] A. Banerjee, K. Damle, and A. Paramekanti, Phys. Rev. B **83**, 134419 (2011).
[76] Y. Tang and A. W. Sandvik, Phys. Rev. Lett. **107**, 157201 (2011).
[77] S. Sanyal, A. Banerjee, and K. Damle, Phys. Rev. B **84**, 235129 (2011).
[78] K. S. D. Beach and A. W. Sandvik, Phys. Rev. Lett. **99**, 047202 (2007).
[79] A. W. Sandvik, Phys. Rev. Lett. **95**, 207203 (2005).
[80] A. W. Sandvik and H. G. Evertz, Phys. Rev. B **82**, 024407 (2010).
[81] H. G. Evertz, G. Lana, and M. Marcu, Phys. Rev. Lett. **70**, 875 (1993).
[82] H. G. Evertz, Adv. Phys. **52**, 1 (2003).
[83] A. W. Sandvik, Phys. Rev. B **59**, R14157 (1999).
[84] K. S. D. Beach and A. W. Sandvik, Nucl. Phys. B **750**, 142 (2006).
[85] N. Kawashima and Y. Tanabe, Phys. Rev. Lett. **98**, 057202 (2007).
[86] N. D. Mermin and H. Wagner, Phys. Rev. Lett. **17**, 1133 (1966).
[87] J. V. Jose, L. P. Kadanoff, S. Kirkpatrick, and D. R. Nelson, Phys. Rev. B **16**, 1217 (1977).
[88] D. Blankschtein, M. Ma, A. N. Berker, G. S. Grest, and C. M. Soukoulis, Phys. Rev. B **29**, 5250 (1984).
[89] M. Caselle and M. Hasenbusch, J. Phys. A **31**, 4603 (1998).
[90] M. Oshikawa, Phys. Rev. B **61**, 3430 (2000).

[91] J. M. Carmona, A. Pelissetto, and E. Vicari, Phys. Rev. B **61**, 15136 (2000).
[92] J. Hove and A. Sudbø, Phys. Rev. E **68**, 046107 (2003).
[93] J. Lou, A. W. Sandvik, and L. Balents, Phys. Rev. Lett. **99**, 207203 (2007).
[94] F. Alet, J. L. Jacobsen, G. Misguich, V. Pasquier, F. Mila, and M. Troyer, Phys. Rev. Lett. **94**, 235702 (2005).
[95] A. B. Kuklov, M. Matsumoto, N. V. Prokofev, B. V. Svistunov, and M. Troyer, Phys. Rev. Lett. **101**, 050405 (2008).
[96] F. Nogueira and A. Sudbø, e-print arXiv:1110.4373.
[97] C. J. Hamer, J. Phys. A **33**, 6683 (2000).
[98] A. Parola, S. Sorella, and Q. F. Zhong, Phys. Rev. Lett. **71**, 4393 (1993).
[99] D. Ihle, C. Schindelin, A. Weisse, and H. Fehske, Phys. Rev. B **60**, 9240 (1999).
[100] A. Sen and A. W. Sandvik, Phys. Rev. B **82**, 174428 (2010).
[101] H.-C. Jiang, H. Yao, and L. Balents (private communication).
[102] M. B. Hastings, I. González, A. B. Kallin, and R. G. Melko, Phys. Rev. Lett. **104**, 157201 (2010).
[103] A. B. Kallin, M. B. Hastings, R. G. Melko, and R. R. P. Singh, Phys. Rev. B **84**, 165134 (2011).
[104] B. Swingle and T. Senthil, e-print arXiv:1109.3185.
[105] Z. Y. Meng, T. C. Lang, S. Wessel, F. F. Assaad, and A. Muramatsu, Nature (London) **464**, 847 (2010).
[106] C. N. Varney, K. Sun, V. Galitski, and M. Rigol, Phys. Rev. Lett. **107**, 077201 (2011).
[107] J. Reuther, D. A. Abanin, and R. Thomale, Phys. Rev. B **84**, 014417 (2011).
[108] A. F. Albuquerque, D. Schwandt, B. Hetényi, S. Capponi, M. Mambrini, and A. M. Läuchli, Phys. Rev. B **84**, 024406 (2011).
[109] F. Mezzacapo and M. Boninsegni, Phys. Rev. B **85**, 060402(R) (2012).
[110] Y. Nishiyama, Phys. Rev. B **85**, 014403 (2012).